Eur. Phys. J. C 29, 215–233 (2003)
Digital Object Identifier (DOI) 10.1140/epjc/s2003-01219-0

THE EUROPEAN PHYSICAL JOURNAL C

Direct CP violation in $B \to \pi^+\pi^- V$ with ρ^0–ω mixing effects: phenomenological approach

Z.J. Ajaltouni[1,a], O. Leitner[1,2,b], P. Perret[1,c], C. Rimbault[1,d], A.W. Thomas[2,e]

[1] Laboratoire de Physique Corpusculaire de Clermont-Ferrand, IN2P3/CNRS Université Blaise Pascal, 63177 Aubière Cedex, France
[2] Department of Physics and Mathematical Physics and Special Research Centre for the Subatomic Structure of Matter, University of Adelaide, Adelaide 5005, Australia

Received: 18 February 2003 / Revised version: 7 April 2003 /
Published online: 23 May 2003 –

Abstract. We present a detailed study of direct CP violation and the branching ratios in the channels $B^{0,\pm} \to \pi^+\pi^- V^{0,\pm}$, where V is a vector meson ($K^{*0,\pm}$ or $\rho^{\pm}$). Emphasis is put upon the important role played by ρ^0–ω mixing effects in the estimation of the CP-violating asymmetry parameter, a_{CP}, associated with the difference of the B and $\bar{B}$ decay amplitudes. A thorough study of the helicity amplitudes is presented as a function of the pion–pion invariant mass. All of the calculations and simulations considered correspond to channels which will be analyzed at the LHCb facility.

1 Introduction

Understanding the physical origin of the violation of CP (charge conjugation × parity) symmetry is one of the main goals of particle physics at the present time. Recent experiments at e^+e^- colliders (BaBar, Belle) have produced fundamental results which strengthen the CKM picture of CP violation [1,2] in the B meson sector [3,4]. However, the main results of these two collaborations are related to B decays into pairs of pseudo-scalar mesons or into a vector plus a pseudo-scalar meson.

A very broad physics program can also be carried out in the sector with two vector mesons in the final state, following B decay. Apart from measuring the *standard angles*, α, β and γ of the unitary triangle (UT), the vector mesons are *polarized* and their decay products (usually long-lived 0^{-+} mesons) are *correlated*. This opens the possibility of making interesting cross-checks of the standard model predictions as well testing some specific models of CP violation beyond the SM approach.

In the special case of two neutral vector mesons, the orbital angular momentum, ℓ, and the total spin, S, of the $V_1^0 V_2^0$ system satisfy the equality $\ell = S = 0, 1, 2$. The CP eigenvalues are defined as $(-1)^{\ell}$. Because of the allowed values for the angular momentum, ℓ, one has a very clear indication of any *mixing* of different CP eigenstates and hence of CP non-conservation. The separation of the different CP eigenstates requires a detailed analysis of the final angular distributions [5]. However, because this analysis can be carried out in a model independent way, it provides a significant constraint on any model.

After explaining the helicity formalism (Sect. 2), a special study is devoted to the final state interactions (FSI) and the key role of ρ^0–ω mixing (Sect. 3). A complete and realistic determination of the helicity amplitudes, in the framework of the effective Hamiltonian approach, is introduced in Sect. 4. Then, the main results of the Monte Carlo simulations, providing estimates of the various density matrix elements h_{ij}, are shown in Sect. 5. In the following section (Sect. 6) the numerical analysis and discussions of the branching ratios and asymmetries for B decays into two vectors ($B \to \rho^0(\omega)V_2$, with $V_2 = K^{*0}, \bar{K}^{*0}, K^{*-}, K^{*+}$, ρ^+, ρ^-) are given in detail. These two vectors, $\rho^0(\omega)$ and V_2, each decay into two pseudo-scalars. Emphasis is put on the angular distributions of the pseudo-scalar mesons in both the helicity and transversity frames. Finally, in the last section, we summarize our results for the different channels which will be investigated in future experiments at pp colliders and make some concluding remarks.

2 General formalism for $B \to V_1 V_2$ decays

2.1 Helicity frame

Because the B meson has spin 0, the final two vector mesons, V_1 and V_2, have the same helicity, $\lambda_1 = \lambda_2 = -1, 0, +1$, and their angular distribution is isotropic in the

[a] e-mail: ziad@clermont.in2p3.fr
[b] e-mail: oleitner@physics.adelaide.edu.au
[c] e-mail: perret@clermont.in2p3.fr
[d] e-mail: rimbault@clermont.in2p3.fr
[e] e-mail: athomas@physics.adelaide.edu.au

B rest frame. Let $H_{\rm w}$ be the weak Hamiltonian which governs the B decays. Any transition amplitude between the initial and final states will have the following form:

$$H_\lambda = \langle V_1(\lambda) V_2(\lambda) | H_{\rm w} | B \rangle \ , \tag{1}$$

where the common helicity is $\lambda = -1, 0, +1$. Then, each vector meson V_i will decay into two pseudo-scalar mesons, a_i, b_i, where a_i and b_i can be either a pion or a kaon, and the angular distributions of a_i and b_i depend on the polarization of V_i.

The helicity frame of a vector meson V_i is defined in the B rest frame such that the direction of the Z-axis is given by its momentum, $\vec{p}_i$. Schematically, the whole process gets the form

$$B \longrightarrow V_1 + V_2 \longrightarrow (a_1 + b_1) + (a_2 + b_2) \ .$$

The corresponding decay amplitude,

$$M_\lambda \left(B \to \sum_{i=1}^{2} (a_i + b_i) \right) ,$$

is factorized out according to the relation

$$\begin{aligned} & M_\lambda \left(B \to \sum_{i=1}^{2} (a_i + b_i) \right) \\ & = H_\lambda (B \to V_1 + V_2) \times \prod_{i=1}^{2} A_i (V_i \to a_i + b_i) \ , \end{aligned} \tag{2}$$

where the amplitudes $A_i(V_i \to a_i + b_i)$ are related to the decay of the resonances V_i. The $A_i(V_i \to a_i + b_i)$ are given by the following expressions:

$$\begin{aligned} A_1(V_1 \to a_1 + b_1) &= \sum_{m_1=-1}^{1} c_1 D^1_{\lambda,m_1}(0, \theta_1, 0) \ , \\ A_2(V_2 \to a_2 + b_2) &= \sum_{m_2=-1}^{1} c_2 D^1_{\lambda,m_2}(\phi, \theta_2, -\phi) \ . \end{aligned} \tag{3}$$

These equalities are an illustration of the Wigner–Eckart theorem. In (3), the c_1 and c_2 parameters represent, respectively, the *dynamical decays* of the V_1 and V_2 resonances. The term $D^1_{\lambda,m_i}(\phi_i, \theta_i, -\phi_i)$ is the Wigner rotation matrix element for a spin-1 particle and we let $\lambda(a_i)$ and $\lambda(b_i)$ be the respective helicities of the final particles a_i and b_i in the V_i rest frame. θ_1 is the polar angle of a_1 in the V_1 helicity frame. The decay plane of V_1 is identified with the $(X$–$Z)$ plane and consequently the azimuthal angle ϕ_1 is set to 0. Similarly, θ_2 and ϕ are respectively the polar and azimuthal angles of particle a_2 in the V_2 helicity frame. Finally, the coefficients m_i are defined by

$$m_i = \lambda(a_i) - \lambda(b_i) \ . \tag{4}$$

Our convention for the $D^1_{\lambda,m_i}(\alpha, \beta, \gamma)$ matrix element is given in Rose's book [6], namely

$$D^1_{\lambda,m_i}(\alpha, \beta, \gamma) = \exp[-{\rm i}(\lambda\alpha + m_i\gamma)] \ d^1_{\lambda,m_i}(\beta) \ . \tag{5}$$

The most general form of the decay amplitude

$$\mathcal{M} \left(B \to \sum_{i=1}^{2} (a_i + b_i) \right)$$

is a *linear superposition* of the previous amplitudes

$$M_\lambda \left(B \to \sum_{i=1}^{2} (a_i + b_i) \right)$$

denoted by

$$\mathcal{M} \left(B \to \sum_{i=1}^{2} (a_i + b_i) \right) = \sum_\lambda M_\lambda \left(B \to \sum_{i=1}^{2} (a_i + b_i) \right) \ . \tag{6}$$

The decay width, $\Gamma(B \to V_1 V_2)$, can be computed by taking the square of the modulus, $\left| \mathcal{M} \left(B \to \sum_{i=1}^{2} (a_i + b_i) \right) \right|$, which involves the three kinematic parameters θ_1, θ_2 and ϕ. This leads to the following general expression:

$$\begin{aligned} & {\rm d}^3\Gamma(B \to V_1 V_2) \\ & \propto \left| \sum_\lambda M_\lambda \left(B \to \sum_{i=1}^{2} (a_i + b_i) \right) \right|^2 \\ & = \sum_{\lambda,\lambda'} h_{\lambda,\lambda'} F_{\lambda,\lambda'}(\theta_1) G_{\lambda,\lambda'}(\theta_2, \phi) \ , \end{aligned} \tag{7}$$

which involves three density matrices, $h_{\lambda,\lambda'}, F_{\lambda,\lambda'}(\theta_1)$ and $G_{\lambda,\lambda'}(\theta_2, \phi)$. The factor $h_{\lambda,\lambda'} = H_\lambda H^*_{\lambda'}$ is an element of the density matrix related to the B decay, while $F_{\lambda,\lambda'}(\theta_1)$ represents the density matrix of the decay $V_1 \to a_1 + b_1$. In a similar way, $G_{\lambda,\lambda'}(\theta_2, \phi)$ represents the density matrix of the decay $V_2 \to a_2 + b_2$.

The analytic expression in (7) exhibits a very general form. It depends on neither the specific nature of the intermediate resonances nor their decay modes (except for the spin of the final particles). This approach also presents three key advantages. The first one comes from the fact that all the dynamics of the B decay is introduced into the coefficients $h_{\lambda,\lambda'}$. This allows us to use various theoretical models involving different dynamical processes and form factors. The second is associated with the fact that the formal expressions for $F_{\lambda,\lambda'}(\theta_1)$ and $G_{\lambda,\lambda'}(\theta_2, \phi)$, which are related to the polarization of the intermediate resonances, remain unchanged whatever the coefficients $h_{\lambda,\lambda'}$ happen to be. Finally, correlations among the final particles arise in a straightforward way because of the previous expression which relates the angles θ_1, θ_2 and ϕ. Consequently, a probability density function (pdf) can be inferred from the general expression, and one gets

$$f(\theta_1, \theta_2, \phi) = \frac{{\rm d}^3\Gamma(B \to V_1 V_2)}{\Gamma(B \to V_1 V_2) {\rm d}(\cos\theta_1) {\rm d}(\cos\theta_2) {\rm d}\phi} \ , \tag{8}$$

where the angles θ_1, θ_2 and ϕ were defined earlier and $\Gamma(B \to V_1 V_2)$ is the partial decay width. This function allows one to compute three other pdfs separately for the variables θ_1, θ_2 and ϕ.

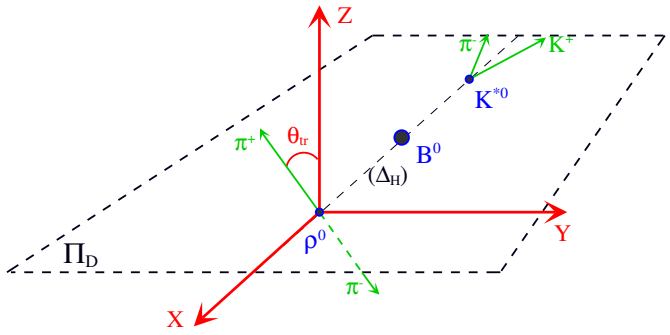

Fig. 1. Transversity frame for $B \to \rho^0 K^*$

The previous calculations are illustrated by the reaction $B^0 \to K^{*0}\rho^0$ where $K^{*0} \to K^+\pi^-$ and $\rho^0 \to \pi^+\pi^-$. In this channel, since all the final particles have spin zero, the coefficients m_1 and m_2, defined in (4), are equal to zero. The three-fold differential width has the following form:

$$\begin{aligned}&\frac{\mathrm{d}^3\Gamma(B \to V_1V_2)}{\mathrm{d}(\cos\theta_1)\mathrm{d}(\cos\theta_2)\mathrm{d}\phi} \qquad (9)\\ &\propto (h_{++} + h_{--})\sin^2\theta_1\sin^2\theta_2/4 + h_{00}\cos^2\theta_1\cos^2\theta_2\\ &+ \Big\{\mathrm{Re}(h_{+0})\cos\phi - \mathrm{Im}(h_{+0})\sin\phi\\ &+ \mathrm{Re}(h_{0-})\cos\phi - \mathrm{Im}(h_{0-})\sin\phi\Big\}\sin 2\theta_1\sin 2\theta_2/4\\ &+ \{\mathrm{Re}(h_{+-})\cos 2\phi - \mathrm{Im}(h_{+-})\sin 2\phi\}\sin^2\theta_1\sin^2\theta_2/2\ ,\end{aligned}$$

where all the terms in (9) have been already specified. It is worth noticing that the expression in (9) is *completely symmetric* in θ_1 and θ_2 and consequently, the angular distributions of a_1 in the V_1 frame is identical that of a_2 in the V_2 frame. From (8) and (9) the normalized pdfs of θ_1, θ_2 and ϕ can be derived and one finds

$$\begin{aligned}f(\cos\theta_{1,2}) &= (3h_{00} - 1)\cos^2\theta_{1,2} + (1 - h_{00})\ , \qquad (10)\\ g(\phi) &= 1 + 2\ \mathrm{Re}(h_{+-})\cos 2\phi - 2\ \mathrm{Im}(h_{+-})\sin 2\phi\ .\end{aligned}$$

2.2 Transversity frame

Initially, the transversity frame (TF) was introduced by Bohr [7] in order to facilitate the determination of the spin and parity of a resonance decaying into stable particles. It can be extended to a system of two vector mesons coming from a heavy meson, B or $\bar{B}$, in order to perform tests of CP symmetry. In displaying new angular distributions, the TF provides physical information complementary to that seen in the standard helicity frame. The construction of the TF and its use require several steps. For a clear illustration, see Fig. 1, where the channel $B^0 \to \rho^0 K^{*0}$ is chosen.

Departing from the B rest frame, the common helicity axis, (Δ_H), is given by the direction of the momentum $\vec{p}_1$. This and the decay plane, (Π_D), of the vector meson $(K^{*0} \to K^+\pi^-)$ are the main ingredients of the TF. The vector meson ρ^0 is taken at rest (origin of the frame) and the X-axis is given by (Δ_H). In the decay plane, (Π_D), the Y-axis, which is orthogonal to the X-axis, is chosen in such a way that the K^+ meson has the Y-component of its momentum greater than or equal to zero. The Z-axis, which is orthogonal to the plane (Π_D), is obtained by the classical relation $\vec{e}_Z = \vec{e}_X \times \vec{e}_Y$.

The angular distributions of the $\pi^\pm$ coming from the ρ^0 decay are referred to the new Z-axis. It is worthy noticing that, in the TF, the flying meson and its decay products are very energetic compared to the B frame. Explicitly, the ρ^0 energy is given by the relation

$$E_{\rho^0} = ({m_B}^2 - {m_1}^2 - {m_2}^2)/2m_1 \approx 17\,\mathrm{GeV}\ , \qquad (11)$$

where m_1 and m_2 refer to the masses of the K^{*0} and ρ^0 resonances, respectively. As far as the transition amplitudes in the TF are concerned, they are a simple linear combination of the helicity amplitudes, namely

$$H_\mathrm{P} = \frac{H_+ + H_-}{\sqrt{2}}\ , \text{ and } H_\mathrm{T} = \frac{H_+ - H_-}{\sqrt{2}}\ , \qquad (12)$$

while H_0 remains unchanged. We can rewrite the angular distributions given in (10) by using the relations from (12) and the angles $\theta_{1,2}, \phi$ expressed in the transversity frame. Thus one gets

$$\begin{aligned}f_\mathrm{T}(\cos\theta_{1,2}) &= \Big(3|H_\mathrm{T}|^2 - 1\Big)\cos^2\theta_{1,2} + \Big(1 - |H_\mathrm{T}|^2\Big)\ ,\\ g_\mathrm{T}(\phi) &= \Big(1 + |H_0|^2 - |H_\mathrm{P}|^2\Big)\cos 2\phi\ . \qquad (13)\end{aligned}$$

3 Final state interactions and ρ^0–ω mixing

3.1 Factorization hypothesis

Final state interactions (FSI) represent unavoidable effects in hadronic physics and they play a crucial role in heavy resonance decays [8]. In the case of a B meson, characterized by a center-of-mass energy $\sqrt{s} \approx 5.3\,\mathrm{GeV}$, the charmless weak decays of the b quark lead to *light energetic* quarks which can exchange several gluons amongst themselves as well as with the spectator quark in the B meson. This fundamental process occurs in decays described by tree, penguin and annihilation diagrams and is characterized by two regimes: the perturbative one and the non-perturbative one. In order to handle the FSI in both regimes, the usual method is inspired by the effective Lagrangian approach. Perturbative calculations at next-to-leading order (NLO) are performed for a scale higher than m_b (since our analysis is focused on B decays) and the non-perturbative effects are inserted for a scale lower than m_b. This general method is called the *factorization procedure* [9] and further details are given below.

In the factorization approximation, either the vector meson $\rho^0(\omega)$ or the K^* is generated by one current in the effective Hamiltonian which has the appropriate quantum numbers. For the B decay processes considered here, two kinds of matrix element products are involved after factorization (i.e. omitting Dirac matrices and color labels):

$$\langle\rho^0(\omega)|(\bar{u}u)|0\rangle\langle K^*|(\bar{q}_i q_j)|B^{\pm,0}\rangle$$

and

$$\langle K^*|(\bar{q}_i q_j)|0\rangle\langle\rho^0(\omega)|(\bar{u}b)|B^{\pm,0}\rangle,$$

where q_i and q_j could be either u, s or d. We will calculate them in two phenomenological quark models.

The matrix elements for $B \to X^*$ (where X^* denotes a vector meson) can be decomposed as follows [10]:

$$\begin{aligned}\langle X^*|J_\mu|B\rangle = {} & \frac{2}{m_B + m_{X^*}}\epsilon_{\mu\nu\rho\sigma}\epsilon^{*\nu}p_B^\rho p_{X^*}^\sigma V(k^2) \\ & + \mathrm{i}\Big\{\epsilon_\mu^*(m_B + m_{X^*})A_1(k^2) \\ & \quad - \frac{\epsilon^*\cdot k}{m_B + m_{X^*}}(P_B + P_{X^*})_\mu A_2(k^2) \\ & \quad - \frac{\epsilon^*\cdot k}{k^2}2m_{X^*}\cdot k_\mu A_3(k^2)\Big\} \\ & + \mathrm{i}\frac{\epsilon^*\cdot k}{k^2}2m_{X^*}\cdot k_\mu A_0(k^2)\ , \end{aligned} \tag{14}$$

where J_μ is the weak current, defined by $J_\mu = \bar{q}\gamma^\mu(1-\gamma_5)b$ with $q = u, d, s$ and $k = p_B - p_{X^*}$ and ϵ_μ is the polarization vector of X^*. The form factors A_0, A_1, A_2, A_3 and V describe the transition $0^- \to 1^-$. Finally, in order to cancel the poles at $q^2 = 0$, the form factors respect the condition

$$A_3(0) = A_0(0)\ , \tag{15}$$

and they also satisfy the following relations:

$$A_3(k^2) = \frac{m_B + m_{X^*}}{2m_{X^*}}A_1(k^2) - \frac{m_B - m_{X^*}}{2m_{X^*}}A_2(k^2)\ . \tag{16}$$

In the evaluation of matrix elements, the effective number of colors, N_c^{eff}, enters through a Fierz transformation. In general, for an operator O_i, one can write

$$\frac{1}{(N_c^{\mathrm{eff}})_i} = \frac{1}{3} + \xi_i\ , \text{with } i = 1, \cdots, 10\ ; \tag{17}$$

here ξ_i describes non-factorizable effects. ξ_i is assumed to be universal for all the operators O_i. Naive factorization assumes that we can replace – in a heavy quark decay – the matrix element of a four fermion operator by the product of the matrix elements of two currents. This reduces to the product of a form factor and a decay constant. This assumption is only rigorously justified at large values of N_c. But it is known that naive factorization may give a good estimate of the magnitude of the B decay amplitude in many cases [11].

3.2 FSI at the quark level: strong phase generated by the penguin diagrams

Let A be the amplitude for the decay $B \to \rho^0(\omega)K^* \to \pi^+\pi^-K^*$ (a similar procedure applies in the case where we have a $\rho^\pm$ [12] instead of the K^*); then one has

$$A = \langle K^*\pi^-\pi^+|H^{\mathrm{T}}|B\rangle + \langle K^*\pi^-\pi^+|H^{\mathrm{P}}|B\rangle\ , \tag{18}$$

with H^{T} and H^{P} being the Hamiltonians for the tree and penguin operators. We can define the relative magnitude and phases between these two contributions as follows:

$$\begin{aligned} A &= \langle K^*\pi^-\pi^+|H^{\mathrm{T}}|B\rangle[1 + r\mathrm{e}^{\mathrm{i}\delta}\mathrm{e}^{\mathrm{i}\phi}]\ , \\ \bar{A} &= \langle \bar{K^*}\pi^+\pi^-|H^{\mathrm{T}}|\bar{B}\rangle[1 + r\mathrm{e}^{\mathrm{i}\delta}\mathrm{e}^{-\mathrm{i}\phi}]\ , \end{aligned} \tag{19}$$

where δ and ϕ are strong and weak phases, respectively. The phase ϕ arises from the appropriate combination of CKM matrix elements, $\phi = \arg[(V_{tb}V_{ts}^*)/(V_{ub}V_{us}^*)]$. As a result, $\sin\phi$ is equal to $\sin\gamma$, with γ defined in the standard way [13]. The parameter r is the absolute value of the ratio of tree and penguin amplitudes:

$$r \equiv \left|\frac{\langle\rho^0(\omega)K^*|H^{\mathrm{P}}|B\rangle}{\langle\rho^0(\omega)K^*|H^{\mathrm{T}}|B\rangle}\right|. \tag{20}$$

3.3 Strong phase generated by the ρ^0–ω mixing

In the vector meson dominance model [14], the photon propagator is dressed by coupling to vector mesons. From this, the ρ^0–ω mixing mechanism [15] was developed. In order to obtain a large signal for direct CP violation, we need some mechanism to make both $\sin\delta$ and r large. We stress that ρ^0–ω mixing has the dual advantages that the strong phase difference is large (passing through 90° at the ω resonance) and well known [12,17]. With this mechanism, to first order in isospin violation, we have the following results when the invariant mass of the $\pi^+\pi^-$ pair is near the mass of the ω resonance:

$$\begin{aligned} \langle K^*\pi^-\pi^+|H^{\mathrm{T}}|B\rangle &= \frac{g_\rho}{s_\rho s_\omega}\tilde{\Pi}_{\rho\omega}t_\omega + \frac{g_\rho}{s_\rho}t_\rho\ , \\ \langle K^*\pi^-\pi^+|H^{\mathrm{P}}|B\rangle &= \frac{g_\rho}{s_\rho s_\omega}\tilde{\Pi}_{\rho\omega}p_\omega + \frac{g_\rho}{s_\rho}p_\rho\ . \end{aligned} \tag{21}$$

Here t_V ($V = \rho$ or ω) is the tree amplitude and p_V the penguin amplitude for producing a vector meson, V; g_ρ is the coupling for $\rho^0 \to \pi^+\pi^-$, $\tilde{\Pi}_{\rho\omega}$ is the effective ρ^0–ω mixing amplitude, and s_V is the inverse propagator of the vector meson V,

$$s_V = s - m_V^2 + \mathrm{i}m_V\Gamma_V\ , \tag{22}$$

with $\sqrt{s}$ being the invariant mass of the $\pi^+\pi^-$ pair. We stress that the direct coupling $\omega \to \pi^+\pi^-$ is effectively absorbed into $\tilde{\Pi}_{\rho\omega}$ [18], leading to the explicit s dependence of $\tilde{\Pi}_{\rho\omega}$. Making the expansion $\tilde{\Pi}_{\rho\omega}(s) = \tilde{\Pi}_{\rho\omega}(m_\omega^2) + (s - m_w^2)\tilde{\Pi}'_{\rho\omega}(m_\omega^2)$, the ρ^0–ω mixing parameters were determined in the fit of Gardner and O'Connell [19]:

$$\begin{aligned} \mathrm{Re}\ \tilde{\Pi}_{\rho\omega}(m_\omega^2) &= -3500 \pm 300\,\mathrm{MeV}^2\ , \\ \mathrm{Im}\ \tilde{\Pi}_{\rho\omega}(m_\omega^2) &= -300 \pm 300\,\mathrm{MeV}^2\ , \end{aligned}$$

and $\tilde{\Pi}'_{\rho\omega}(m_\omega^2) = 0.03 \pm 0.04$. In practice, the effect of the derivative term is negligible. From (18) and (21) one has

$$r\mathrm{e}^{\mathrm{i}\delta}\mathrm{e}^{\mathrm{i}\phi} = \frac{\tilde{\Pi}_{\rho\omega}p_\omega + s_\omega p_\rho}{\tilde{\Pi}_{\rho\omega}t_\omega + s_\omega t_\rho}\ . \tag{23}$$

Defining

$$\frac{p_\omega}{t_\rho} \equiv r' \mathrm{e}^{\mathrm{i}(\delta_q+\phi)} \ , \quad \frac{t_\omega}{t_\rho} \equiv \alpha \mathrm{e}^{\mathrm{i}\delta_\alpha} \ , \quad \frac{p_\rho}{p_\omega} \equiv \beta \mathrm{e}^{\mathrm{i}\delta_\beta} \ , \quad (24)$$

where $\delta_\alpha, \delta_\beta$ and δ_q are partial strong phases (absorptive part) arising from the tree and penguin diagram contributions. Substituting (24) into (23), one finds

$$r\mathrm{e}^{\mathrm{i}\delta} = r' \mathrm{e}^{\mathrm{i}\delta_q} \frac{\tilde{\Pi}_{\rho\omega} + \beta \mathrm{e}^{\mathrm{i}\delta_\beta} s_\omega}{s_\omega + \tilde{\Pi}_{\rho\omega} \alpha \mathrm{e}^{\mathrm{i}\delta_\alpha}} \ , \quad (25)$$

where the total strong phase, δ, is mainly proportional to the ratio of the penguin and tree diagram contributions.

3.4 Importance of the strong phase for $B\bar{B}$ asymmetry

Under a CP transformation the strong phase, δ, remains unchanged, while the weak phase, ϕ, which is related to the CKM matrix elements, changes sign. Thus, the asymmetry parameter, a_{CP}^{dir}, which can reveal *direct CP violation*, can be deduced in the following way:

$$a_{CP}^{\mathrm{dir}} = \frac{A^2 - \bar{A}^2}{A^2 + \bar{A}^2} = \frac{-2\ r\ \sin\delta\ \sin\phi}{1 + r^2 + 2\ r\ \cos\delta\ \cos\phi} \ . \quad (26)$$

It is straightforward to see that the parameter a_{CP}^{dir} depends on both the strong phase *and* the weak phase and, consequently, that the maximum value of a_{CP}^{dir} can be reached if $\sin\delta = 1$. This is why the strong final state interaction (FSI) among pions coming from ρ^0–ω mixing *enhances* the direct CP violation in the vicinity of the mass of the ω resonance.

In the Wolfenstein parameterization [20], the weak phase comes from $[V_{tb}V_{ts}^*/V_{ub}V_{us}^*]$ and one has for the decay $B \to \rho^0(\omega)K^*$,

$$\sin\phi = \frac{-\eta}{\sqrt{\rho^2+\eta^2}} \ , \quad \cos\phi = \frac{-\rho}{\sqrt{\rho^2+\eta^2}} \ , \quad (27a)$$

while the weak phase comes from $[V_{tb}V_{td}^*/V_{ub}V_{ud}^*]$ for the decay $B \to \rho^0(\omega)\rho$,

$$\sin\phi = \frac{\eta}{\sqrt{[\rho(1-\rho)-\eta^2]^2+\eta^2}} \ , \quad \cos\phi = \frac{\rho(1-\rho)-\eta^2}{\sqrt{[\rho(1-\rho)-\eta^2]^2+\eta^2}} \ . \quad (27b)$$

The values used for ρ and η will be discussed in Sect. 5.

4 Explicit calculations according to the effective Hamiltonian

4.1 Generalities concerning the OPE for weak hadronic decays

4.1.1 Operator product expansion

The operator product expansion (OPE) [21] is an extremely useful tool in the analysis of weak interaction processes involving quarks. Defining the decay amplitude $A(M \to F)$ as

$$A(M \to F) \propto C_i(\mu) \langle F | O_i(\mu) | M \rangle \ , \quad (28)$$

where $C_i(\mu)$ are the Wilson coefficients (see Sect. 4.1.2), $O_i(\mu)$ are the operators given by the OPE and μ is an energy scale, one sees that the OPE separates the calculation of the amplitude, $A(M \to F)$, into two distinct physical regimes. One is related to *hard* or short-distance physics, represented by $C_i(\mu)$ and calculated by a perturbative approach. The other is the *soft* or long-distance regime. This part must be treated by non-perturbative approaches such as the $1/N$ expansion [22], QCD sum rules [23], hadronic sum rules or lattice QCD.

The operators, O_i, are local operators which can be written in the general form:

$$O_i = (\bar{q}_i \Gamma_{n1} q_j)(\bar{q}_k \Gamma_{n2} q_l) \ , \quad (29)$$

where Γ_{n1} and Γ_{n2} denote a combination of gamma matrices and q the quark flavor. They should respect the Dirac structure, the color structure and the types of quarks relevant for the decay being studied. They can be divided into two classes according to topology: tree operators (O_1, O_2), and penguin operators (O_3 to O_{10}). For tree contributions (where $W^\pm$ is exchanged), the Feynman diagram is shown in Fig. 2 (left). The current–current operators related to the tree diagram are the following:

$$O_1^s = \bar{q}_\alpha \gamma_\mu (1-\gamma_5) u_\beta \bar{s}_\beta \gamma^\mu (1-\gamma_5) b_\alpha \ , \quad O_2^s = \bar{q} \gamma_\mu (1-\gamma_5) u \bar{s} \gamma^\mu (1-\gamma_5) b \ , \quad (30)$$

where α and β are the color indices. The penguin terms can be divided into two sets. The first is from the QCD penguin diagrams where gluons are exchanged, while the second is from the electroweak penguin diagrams (where either a γ or a Z^0 is exchanged). The Feynman diagram for the QCD penguin diagram is shown in Fig. 2 (right) and the corresponding operators are written as follows:

$$O_3 = \bar{q}\gamma_\mu(1-\gamma_5) b \sum_{q'} \bar{q}'\gamma^\mu(1-\gamma_5) q' \ , \quad O_4 = \bar{q}_\alpha \gamma_\mu (1-\gamma_5) b_\beta \sum_{q'} \bar{q}'_\beta \gamma^\mu (1-\gamma_5) q'_\alpha \ , \quad (31a)$$

$$O_5 = \bar{q}\gamma_\mu(1-\gamma_5) b \sum_{q'} \bar{q}'\gamma^\mu(1+\gamma_5) q' \ , \quad O_6 = \bar{q}_\alpha \gamma_\mu (1-\gamma_5) b_\beta \sum_{q'} \bar{q}'_\beta \gamma^\mu (1+\gamma_5) q'_\alpha \ , \quad (31b)$$

where $q' = u, d, s, c$. Finally, the electroweak penguin operators arise from the two Feynman diagrams represented in Fig. 3 (left) and Fig. 3 (right) where Z, γ are exchanged from a quark line and from the W line, respectively. They have the following expressions:

$$O_7 = \frac{3}{2} \bar{q}\gamma_\mu(1-\gamma_5) b \sum_{q'} e_{q'} \bar{q}'\gamma^\mu(1+\gamma_5) q' \ ,$$

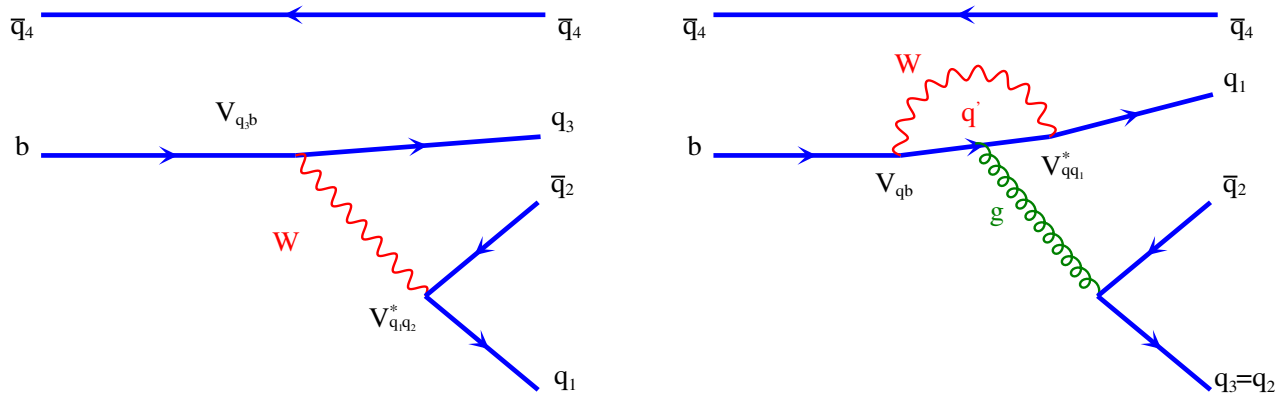

Fig. 2. Tree diagram (*left*), and QCD penguin diagram (*right*), for B decays

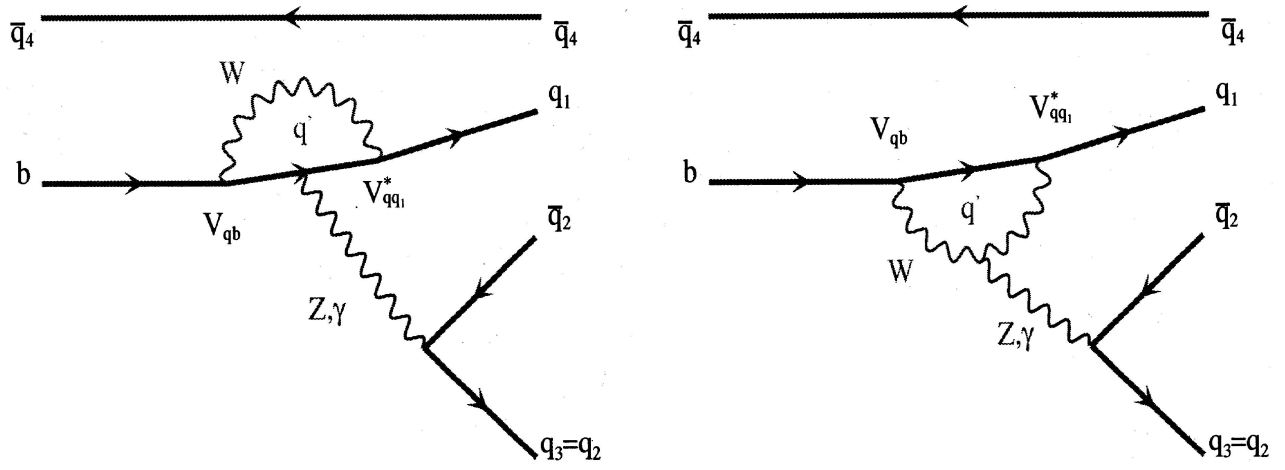

Fig. 3. Electroweak penguin diagram (*left*), and electroweak penguin diagram with coupling between Z, γ and W (*right*), for B decays

$$O_8 = \frac{3}{2}\bar{q}_\alpha\gamma_\mu(1-\gamma_5)b_\beta \sum_{q'} e_{q'}\bar{q}'_\beta\gamma^\mu(1+\gamma_5)q'_\alpha \ ,$$
$$O_9 = \frac{3}{2}\bar{q}\gamma_\mu(1-\gamma_5)b \sum_{q'} e_{q'}\bar{q}'\gamma^\mu(1-\gamma_5)q' \ , \qquad (32)$$
$$O_{10} = \frac{3}{2}\bar{q}_\alpha\gamma_\mu(1-\gamma_5)b_\beta \sum_{q'} e_{q'}\bar{q}'_\beta\gamma^\mu(1-\gamma_5)q'_\alpha \ ,$$

where $e_{q'}$ denotes the electric charge of q'.

4.1.2 Wilson coefficients

As we mentioned in the preceding subsection, the Wilson coefficients [24], $C_i(\mu)$, represent the physical contributions from scales higher than μ (the OPE describes physics for scales lower than μ). Since QCD has the property of asymptotic freedom, they can be calculated in perturbation theory. The Wilson coefficients include the contributions of all heavy particles, such as the top quark, the W bosons, and the charged Higgs boson. Usually, the scale μ is chosen to be of $\mathcal{O}(m_b)$ for B decays. The Wilson coefficients have been calculated to next-to-leading order (NLO). The evolution of $C(\mu)$ (the matrix that includes $C_i(\mu)$) is given by

$$C(\mu) = U(\mu, M_W)C(M_W) \ , \qquad (33)$$

where $U(\mu, M_W)$ is the QCD evolution matrix:

$$U(\mu, M_W) = \left[1 + \frac{\alpha_s(\mu)}{4\pi}J\right] \times U^0(\mu, M_W)\left[1 - \frac{\alpha_s(M_W)}{4\pi}J\right] \ , \qquad (34)$$

with J the matrix summarizing the next-to-leading order corrections and $U^0(\mu, M_W)$ the evolution matrix in the leading-logarithm approximation. Since the strong interaction is independent of quark flavor, the $C(\mu)$ are the same for all B decays. At the scale $\mu = m_b = 5\,\mathrm{GeV}$, $C(\mu)$ take the values summarized in Table 1. To be consistent, the matrix elements of the operators, O_i, should also be renormalized to the one-loop order. This results in the effective Wilson coefficients, C'_i, which satisfy the constraint

$$C_i(m_b)\langle O_i(m_b)\rangle = C'_i\langle O_i\rangle^{\mathrm{tree}} \ ; \qquad (35)$$

here $\langle O_i\rangle^{\mathrm{tree}}$ are the matrix elements at the tree level. These matrix elements will be evaluated within the factorization approach. From (35), the relations between C'_i and C_i are [25,26]

Table 1. Wilson coefficients to the next-leading order (see the reference in text)

$C_i(\mu)$ for $\mu = 5\,\mathrm{GeV}$			
	C_1	-0.3125	
	C_2	$+1.1502$	
C_3	$+0.0174$	C_5	$+0.0104$
C_4	-0.0373	C_6	-0.0459
C_7	-1.050×10^{-5}	C_9	-0.0101
C_8	$+3.839 \times 10^{-4}$	C_{10}	$+1.959 \times 10^{-3}$

$$\begin{aligned} C'_1 &= C_1 \ , & C'_2 &= C_2 \ , \\ C'_3 &= C_3 - P_s/3 \ , & C'_4 &= C_4 + P_s \ , \\ C'_5 &= C_5 - P_s/3 \ , & C'_6 &= C_6 + P_s \ , \\ C'_7 &= C_7 + P_e \ , & C'_8 &= C_8 \ , \\ C'_9 &= C_9 + P_e \ , & C'_{10} &= C_{10} \ , \end{aligned} \tag{36}$$

where

$$\begin{aligned} P_s &= (\alpha_\mathrm{s}/8\pi)C_2(10/9 + G(m_c, \mu, q^2)) \ , \\ P_e &= (\alpha_\mathrm{em}/9\pi)(3C_1 + C_2)(10/9 + G(m_c, \mu, q^2)) \ , \end{aligned} \tag{37}$$

and

$$G(m_c, \mu, q^2) = 4\int_0^1 \mathrm{d}x \ x(x-1)\ln\frac{m_c^2 - x(1-x)q^2}{\mu^2} \ . \tag{38}$$

Here q^2 is the typical momentum transfer of the gluon or photon in the penguin diagrams and $G(m_c, \mu, q^2)$ has the following explicit expression [27]:

$$\begin{aligned} \mathrm{Re}\ G = \frac{2}{3}\Bigg(&\ln\frac{m_c^2}{\mu^2} - \frac{5}{3} - 4\frac{m_c^2}{q^2} \\ &+ \left(1 + 2\frac{m_c^2}{q^2}\right)\sqrt{1 - 4\frac{m_c^2}{q^2}}\ln\frac{1 + \sqrt{1 - 4\frac{m_c^2}{q^2}}}{1 - \sqrt{1 - 4\frac{m_c^2}{q^2}}}\Bigg) , \\ \mathrm{Im}\ G = -\frac{2}{3}&\left(1 + 2\frac{m_c^2}{q^2}\right)\sqrt{1 - 4\frac{m_c^2}{q^2}} \ . \end{aligned} \tag{39}$$

Based on simple arguments at the quark level, the value of q^2 is chosen in the range $0.3 < q^2/m_b^2 < 0.5$ [12,28]. From (36)–(39) we can obtain numerical values for C'_i. These values are listed in Table 2, where we have taken $\alpha_\mathrm{s}(m_Z) = 0.112$, $\alpha_\mathrm{em}(m_b) = 1/132.2$, $m_b = 5\,\mathrm{GeV}$, and $m_c = 1.35\,\mathrm{GeV}$.

4.1.3 Effective Hamiltonian

In any phenomenological treatment of the weak decays of hadrons, the starting point is the weak effective Hamiltonian at low energy [29]. It is obtained by integrating out the heavy fields (e.g. the top quark, W and Z bosons) from the standard model Lagrangian. It can be written as

$$\mathcal{H}_\mathrm{eff} = \frac{G_\mathrm{F}}{\sqrt{2}}\sum_i V_\mathrm{CKM} C_i(\mu) O_i(\mu) \ , \tag{40}$$

where G_F is the Fermi constant, V_CKM is the CKM matrix element (see Sect. 4.3), $C_i(\mu)$ are the Wilson coefficients (see Sect. 4.1.2), $O_i(\mu)$ are the operators from the operator product expansion (see Sect. 4.1.1), and μ represents the renormalization scale. We emphasize that the amplitude corresponding to the effective Hamiltonian for a given decay is independent of the scale μ. In the present case, since we analyze direct CP violation in B decays, we take into account both tree and penguin diagrams. For the penguin diagrams, we include all operators O_3 to O_{10}. Therefore, the effective Hamiltonian used will be

$$\begin{aligned} \mathcal{H}_\mathrm{eff}^{\triangle B=1} = \frac{G_\mathrm{F}}{\sqrt{2}}&\left[V_{ub}V_{us}^*(C_1 O_1^s + C_2 O_2^s) - V_{tb}V_{ts}^*\sum_{i=3}^{10} C_i O_i\right] \\ &+ \mathrm{H.c.} \ , \end{aligned} \tag{41}$$

and consequently, the decay amplitude can be expressed as follows:

$$\begin{aligned} &A(B \to V_1 V_2) \\ &= \frac{G_\mathrm{F}}{\sqrt{2}}\Bigg[V_{ub}V_{us}^*\left(C_1\langle V_1V_2|O_1^s|B\rangle + C_2\langle V_1V_2|O_2^s|B\rangle\right) \\ &- V_{tb}V_{ts}^*\sum_{i=3}^{10} C_i\langle V_1V_2|O_i|B\rangle\Bigg] + \mathrm{H.c.} \ , \end{aligned} \tag{42}$$

where $\langle V_1V_2|O_i|B\rangle$ are the hadronic matrix elements. They describe the transition between the initial state and the final state for scales lower than μ and include, up to now, the main uncertainties in the calculation since they involve non-perturbative effects.

4.2 New expression of helicity amplitudes h_{ij} according to Wilson coefficients

4.2.1 General helicity amplitude

The weak hadronic matrix element is expressed as the sum of three helicity matrix elements, each of which takes the form $H_\lambda\left(B \to \rho^0(\omega)V_2\right) = \langle V_1V_2|{H_\mathrm{w}}^\mathrm{eff}|B\rangle$, and is defined by gathering all the Wilson coefficients of both the tree and penguin operators. Linear combinations of those coefficients arise, such as $c_{t_i}^{V_i}$ (tree diagram contribution) and $c_{p_i}^{V_i}$ (penguin diagram contribution). Then, in the case of $B \to \rho^0(\omega)V_2$, ($V_1 = \rho^0$ or ω), the helicity amplitude $H_\lambda\left(B \to \rho^0(\omega)V_2\right)$ has the general following expression:

$$\begin{aligned} &H_\lambda\left(B \to \rho^0(\omega)V_2\right) \\ &= \left(V_{ub}V_{us}^* c_{t_1}^\rho - V_{tb}V_{ts}^* c_{p_1}^\rho\right) \\ &\times \Big\{\beta_1^\rho \varepsilon_{\alpha\beta\gamma\delta}\epsilon_{V_2}^{*\alpha}(\lambda)\epsilon_\rho^{*\beta}(\lambda)P_B^\gamma P_{V_2}^\delta \\ &+ \mathrm{i}\left(\beta_2^\rho \epsilon_{V_2}^*(\lambda)\epsilon_\rho^*(\lambda) - \beta_3^\rho(\epsilon_{V_2}^*(\lambda)\cdot P_B)(\epsilon_\rho^*(\lambda)\cdot P_B)\right)\Big\} \\ &+ \left(V_{ub}V_{us}^* c_{t_2}^\rho - V_{tb}V_{ts}^* c_{p_2}^\rho\right) \\ &\times \Big\{\beta_4^\rho \varepsilon_{\alpha\beta\gamma\delta}\epsilon_\rho^{*\alpha}(\lambda)\epsilon_{V_2}^{*\beta}(\lambda)P_B^\gamma P_\rho^\delta \end{aligned}$$

Table 2. Effective Wilson coefficients related to the tree operators, electroweak and QCD penguin operators (see the reference in text)

C'_i	$q^2/m_b^2 = 0.3$	$q^2/m_b^2 = 0.5$
C'_1	-0.3125	-0.3125
C'_2	$+1.1502$	$+1.1502$
C'_3	$+2.433 \times 10^{-2} + 1.543 \times 10^{-3}\mathrm{i}$	$+2.120 \times 10^{-2} + 2.174 \times 10^{-3}\mathrm{i}$
C'_4	$-5.808 \times 10^{-2} - 4.628 \times 10^{-3}\mathrm{i}$	$-4.869 \times 10^{-2} - 1.552 \times 10^{-2}\mathrm{i}$
C'_5	$+1.733 \times 10^{-2} + 1.543 \times 10^{-3}\mathrm{i}$	$+1.420 \times 10^{-2} + 5.174 \times 10^{-3}\mathrm{i}$
C'_6	$-6.668 \times 10^{-2} - 4.628 \times 10^{-3}\mathrm{i}$	$-5.729 \times 10^{-2} - 1.552 \times 10^{-2}\mathrm{i}$
C'_7	$-1.435 \times 10^{-4} - 2.963 \times 10^{-5}\mathrm{i}$	$-8.340 \times 10^{-5} - 9.938 \times 10^{-5}\mathrm{i}$
C'_8	$+3.839 \times 10^{-4}$	$+3.839 \times 10^{-4}$
C'_9	$-1.023 \times 10^{-2} - 2.963 \times 10^{-5}\mathrm{i}$	$-1.017 \times 10^{-2} - 9.938 \times 10^{-5}\mathrm{i}$
C'_{10}	$+1.959 \times 10^{-3}$	$+1.959 \times 10^{-3}$

$$
\begin{aligned}
&+ \mathrm{i}\left(\beta_5^\rho \epsilon_\rho^*(\lambda)\epsilon_{V_2}^*(\lambda) - \beta_6^\rho(\epsilon_\rho^*(\lambda)\cdot P_B)(\epsilon_{V_2}^*(\lambda)\cdot P_B)\right)\Big\} \\
&+ \frac{\tilde{\Pi}_{\rho\omega}}{(s_\rho - m_\omega^2) + \mathrm{i}m_\omega\Gamma_\omega}\Bigg[\left(V_{ub}V_{us}^* c_{t_1}^\omega - V_{tb}V_{ts}^* c_{p_1}^\omega\right) \\
&\times \Big\{\beta_1^\omega \varepsilon_{\alpha\beta\gamma\delta}\epsilon_{V_2}^{*\alpha}(\lambda)\epsilon_\omega^{*\beta}(\lambda)P_B^\gamma P_{V_2}^\delta \\
&+ \mathrm{i}\left(\beta_2^\omega \epsilon_{V_2}^*(\lambda)\epsilon_\omega^*(\lambda) - \beta_3^\omega(\epsilon_{V_2}^*(\lambda)\cdot P_B)(\epsilon_\omega^*(\lambda)\cdot P_B)\right)\Big\} \\
&+ \left(V_{ub}V_{us}^* c_{t_2}^\omega - V_{tb}V_{ts}^* c_{p_2}^\omega\right) \\
&\times \Big\{\beta_4^\omega \varepsilon_{\alpha\beta\gamma\delta}\epsilon_\omega^{*\alpha}(\lambda)\epsilon_{V_2}^{*\beta}(\lambda)P_B^\gamma P_\omega^\delta + \mathrm{i}\Big(\beta_5^\omega \epsilon_\omega^*(\lambda)\epsilon_{V_2}^*(\lambda) \\
&- \beta_6^\omega(\epsilon_\omega^*(\lambda)\cdot P_B)(\epsilon_{V_2}^*(\lambda)\cdot P_B)\Big)\Big\}\Bigg] , \qquad (43)
\end{aligned}
$$

with $\epsilon_{V_2,\rho,\omega}(\lambda)$ being the K^*, ρ^0 and ω polarization vectors expressed in the B rest frame. Finally $\varepsilon_{\alpha\beta\gamma\delta}$ is the antisymmetric tensor in Minkowski space.

In (43) the parameters β_i are mainly the form factors describing transitions between vector mesons. They take the form

$$
\begin{aligned}
\beta_{1,4}^{V_1} &= \frac{G_\mathrm{F}}{2} f_{V_1,V_2} m_{V_1,V_2} \\
&\quad \times \frac{2}{m_B + m_{V_2,V_1}} V^{B\to V_2,V_1}(m_{V_1,V_2}^2) , \qquad (44) \\
\beta_{2,5}^{V_1} &= \frac{G_\mathrm{F}}{2} f_{V_1,V_2} m_{V_1,V_2} \\
&\quad \times (m_B + m_{V_2,V_1}) A_1^{B\to V_2,V_1}(m_{V_1,V_2}^2) , \qquad (45) \\
\beta_{3,6}^{V_1} &= \frac{G_\mathrm{F}}{2} f_{V_1,V_2} m_{V_1,V_2} \\
&\quad \times \frac{2}{m_B + m_{V_2,V_1}} A_2^{B\to V_2,V_1}(m_{V_1,V_2}^2) ; \qquad (46)
\end{aligned}
$$

here f_{V_1,V_2} is either the ρ^0, ω or the K^* decay constant. $V^{B\to V_2,V_1}$ and $A_i^{B\to V_2,V_1}$ are respectively the vector and axial form factors defined in (14)–(16). It is worth noticing that the tensorial terms which enter $H_\lambda\left(B \to \rho^0(\omega)V_2\right)$ become simplified in the B rest frame because the four-momentum of the B is given by $P_B = (m_B, \vec{0})$. Then, using the orthogonality properties of $\epsilon_{V_i}(\lambda)$, the helicity amplitude $H_\lambda\left(B \to \rho^0(\omega)V_2\right)$ acquires a much simpler expression than above:

$$
\begin{aligned}
&H_\lambda\left(B \to \rho^0(\omega)V_2\right) \\
&= \mathrm{i}B_\lambda^\rho(V_{ub}V_{us}^* c_{t_1}^\rho - V_{tb}V_{ts}^* c_{p_1}^\rho) \\
&+ \mathrm{i}C_\lambda^\rho(V_{ub}V_{us}^* c_{t_2}^\rho - V_{tb}V_{ts}^* c_{p_2}^\rho) \\
&+ \frac{\tilde{\Pi}_{\rho\omega}}{(s_\rho - m_\omega^2) + \mathrm{i}m_\omega\Gamma_\omega}\Big[\mathrm{i}B_\lambda^\omega(V_{ub}V_{us}^* c_{t_1}^\omega - V_{tb}V_{ts}^* c_{p_1}^\omega) \\
&\quad + \mathrm{i}C_\lambda^\omega(V_{ub}V_{us}^* c_{t_2}^\omega - V_{tb}V_{ts}^* c_{p_2}^\omega)\Big] , \qquad (47)
\end{aligned}
$$

where the terms $B_\lambda^{V_1}$ and $C_\lambda^{V_1}$ take the following forms for the helicity (λ) values $-1, 0, +1$:

$$
\begin{aligned}
B_{\lambda=0}^{V_1} &= \beta_2^{V_1}\frac{m_B^2 - (m_{V_2}^2 + m_{V_1}^2)}{2m_{V_2}m_{V_1}} - \beta_3^{V_1}\frac{|\vec{p}|^2 m_B^2}{m_{V_2}m_{V_1}} , \qquad (48) \\
C_{\lambda=0}^{V_1} &= \beta_5^{V_1}\frac{m_B^2 - (m_{V_2}^2 + m_{V_1}^2)}{2m_{V_2}m_{V_1}} - \beta_6^{V_1}\frac{|\vec{p}|^2 m_B^2}{m_{V_2}m_{V_1}} , \qquad (49) \\
B_{\lambda=\pm1}^{V_1} &= \mp\beta_1^{V_1} m_B|\vec{p}| - \beta_2^{V_1} , \qquad (50) \\
C_{\lambda=\pm1}^{V_1} &= \mp\beta_4^{V_1} m_B|\vec{p}| - \beta_5^{V_1} . \qquad (51)
\end{aligned}
$$

In the above equations, $|\vec{p}|$ is the momentum common to the V_1 and V_2 particles in the B rest frame. It takes the form

$$
|\vec{p}| = \frac{\sqrt{[m_B^2 - (m_{V_1} + m_{V_2})^2][m_B^2 - (m_{V_1} - m_{V_2})^2]}}{2m_B} , \qquad (52)
$$

where m_1 and m_2 are the vector masses. Taking into account the previous relations, we arrive at the final form for the amplitudes $H_\lambda\left(B \to \rho^0(\omega)V_2\right)$:

$$
\begin{aligned}
&H_{\lambda=^0_{\pm1}}\left(B \to \rho^0(\omega)V_2\right) \\
&= A\lambda^2\Big\{\left[R_1^\rho B_{\lambda=^0_{\pm1}}^\rho + R_2^\rho C_{\lambda=^0_{\pm1}}^\rho\right] \\
&+ \mathrm{i}\left[I_1^\rho B_{\lambda=^0_{\pm1}}^\rho + I_2^\rho C_{\lambda=^0_{\pm1}}^\rho\right]\Big\} + \frac{\tilde{\Pi}_{\rho\omega}}{(s_\rho - m_\omega^2) + \mathrm{i}m_\omega\Gamma_\omega}
\end{aligned}
$$

$$\times \left[A\lambda^2 \left\{ \left[R_1^\omega B^\omega_{\lambda=^0_{\pm 1}} + R_2^\omega C^\omega_{\lambda=^0_{\pm 1}} \right] + \mathrm{i} \left[I_1^\omega B^\omega_{\lambda=^0_{\pm 1}} + I_2^\omega C^\omega_{\lambda=^0_{\pm 1}} \right] \right\} \right] , \quad (53)$$

where one defines

$$R_i^{V_1} = \eta\lambda^2 c_{t_i}^{V_1} - \mathrm{Im}(c_{p_i}^{V_1}) , \quad (54)$$

$$I_i^{V_1} = \rho\lambda^2 c_{t_i}^{V_1} + \mathrm{Re}(c_{p_i}^{V_1}) , \quad (55)$$

with V_1 being either ρ^0 or ω. From (53), the density matrix elements $h_{\lambda,\lambda'}$ can be derived automatically, and one has

$$h_{\lambda,\lambda'} = H_\lambda \left(B \to \rho^0(\omega) V_2 \right) H^*_{\lambda'} \left(B \to \rho^0(\omega) V_2 \right) . \quad (56)$$

Because of the hermiticity of the matrix $(h_{\lambda,\lambda'})$, only six elements must be calculated.

4.2.2 Explicit amplitudes for the B decays investigated

By applying the formalism described in Sect. 3, one gets in the case of the ρ^0 production the following linear combinations of the effective Wilson coefficients.

(1) For the decay $\bar{B}^0 \to \bar{K}^{*0}\rho^0$:

$$c^\rho_{t_1} = C'_1 + \frac{C'_2}{N_c} , \quad c^\rho_{p_1} = \frac{3}{2}\left(C'_9 + \frac{C'_{10}}{N_c} + C'_7 + \frac{C'_8}{N_c} \right) ,$$
$$c^\rho_{t_2} = 0 , \quad c^\rho_{p_2} = -\left(C'_4 + \frac{C'_3}{N_c} \right) + \frac{1}{2}\left(C'_{10} + \frac{C'_9}{N_c} \right) , \quad (57a)$$

where the C'_i are listed in Table 2. The coefficients $c^\rho_{t_i}$ relate to the tree diagrams and $c^\rho_{p_i}$ to the penguin diagrams. To simplify the formulas we used N_c for N_c^{eff} in the expressions (57a)–(57d).

(2) For the decay $B^- \to K^{*-}\rho^0$:

$$c^\rho_{t_1} = C'_1 + \frac{C'_2}{N_c} , \quad c^\rho_{p_1} = \frac{3}{2}\left(C'_9 + \frac{C'_{10}}{N_c} + C'_7 + \frac{C'_8}{N_c} \right) ,$$
$$c^\rho_{t_2} = C'_2 + \frac{C'_1}{N_c} , \quad c^\rho_{p_2} = C'_4 + \frac{C'_3}{N_c} + C'_{10} + \frac{C'_9}{N_c} . \quad (57b)$$

In the case of ω production one obtains the following linear combinations of effective Wilson coefficients.

(1) For the decay $\bar{B}^0 \to \bar{K}^{*0}\omega$:

$$c^\omega_{t_1} = 0 , \quad c^\omega_{p_1} = -C'_4 - \frac{C'_3}{N_c} + \frac{1}{2}\left(C'_{10} + \frac{C'_9}{N_c} \right) ,$$
$$c^\omega_{t_2} = C'_1 + \frac{C'_2}{N_c} ,$$
$$c^\omega_{p_2} = 2\left(C'_3 + \frac{C'_4}{N_c} + C'_5 + \frac{C'_6}{N_c} \right) + \frac{1}{2}\left(C'_9 + \frac{C'_{10}}{N_c} + C'_7 + \frac{C'_8}{N_c} \right) . \quad (57c)$$

(2) For the decay $B^- \to K^{*-}\omega$:

$$c^\omega_{t_1} = C'_2 + \frac{C'_1}{N_c} , \quad c^\omega_{p_1} = C'_4 + \frac{C'_3}{N_c} + \left(C'_{10} + \frac{C'_9}{N_c} \right) ,$$
$$c^\omega_{t_2} = C'_1 + \frac{C'_2}{N_c} ,$$
$$c^\omega_{p_2} = 2\left(C'_3 + \frac{C'_4}{N_c} + C'_5 + \frac{C'_6}{N_c} \right) + \frac{1}{2}\left(C'_9 + \frac{C'_{10}}{N_c} + C'_7 + \frac{C'_8}{N_c} \right) . \quad (57d)$$

We refer to Appendix A for details of the helicity amplitudes, while for the channel $B^\pm \to \rho^0(\omega)\rho^\pm$ we refer to Appendix B.

4.3 CKM matrix and form factors

In phenomenological applications, the widely used representation of the CKM matrix is the *Wolfenstein parametrization* [20]. In this approach, the four independent parameters are λ_c, A, ρ and η. Then, by expanding each element of the matrix as a power series in the parameter $\lambda_c = \sin\theta_c = 0.2209$ (θ_c is the Gell-Mann–Levy–Cabibbo angle), one finds ($O(\lambda_c^4)$ is neglected)

$$\hat{V}_{\mathrm{CKM}} = \begin{pmatrix} 1 - \frac{1}{2}\lambda_c^2 & \lambda_c & A\lambda_c^3(\rho - \mathrm{i}\eta) \\ -\lambda_c & 1 - \frac{1}{2}\lambda_c^2 & A\lambda_c^2 \\ A\lambda_c^3(1 - \rho - \mathrm{i}\eta) & -A\lambda_c^2 & 1 \end{pmatrix} , \quad (58)$$

where η plays the role of the CP-violating phase. In this parametrization, even though it is an approximation in λ_c, the CKM matrix satisfies unitarity exactly, which means that

$$\hat{V}^\dagger_{\mathrm{CKM}} \cdot \hat{V}_{\mathrm{CKM}} = \hat{I} = \hat{V}_{\mathrm{CKM}} \cdot \hat{V}^\dagger_{\mathrm{CKM}} . \quad (59)$$

The form factors, $V(k^2)$ and $A_j(k^2)$, depend on the inner structure of the hadrons. Here we will adopt two different theoretical approaches. The first was proposed by Bauer, Stech, and Wirbel [10] (BSW), who used the overlap integrals of wave functions in order to evaluate the meson–meson matrix elements of the corresponding current. In that case the momentum dependence of the form factors is based on a single-pole ansatz. The second approach was developed by Guo and Huang (GH) [30], who modified the BSW model by using some wave functions described in the light-cone framework. Nevertheless, both of these models use phenomenological form factors which are parameterized by making the assumption of nearest pole dominance. The explicit k^2 dependence of the form factor is [10,31]:

$$V(k^2) = \frac{h_V}{\left(1 - \frac{k^2}{m_V^2}\right)} , \quad A_j(k^2) = \frac{h_{A_j}}{\left(1 - \frac{k^2}{m_{A_j}^2}\right)} , \quad (60)$$

where m_{A_j} and m_V are the pole masses associated with the transition current and h_V and h_{A_j} are the values of the form factors at $q^2 = 0$.

5 Monte Carlo simulations: computation of h_{ij} and general results

5.1 Numerical inputs

5.1.1 CKM values

In our numerical calculations we have several parameters: $q^2, N_c^{\rm eff}$ and the CKM matrix elements in the Wolfenstein parametrization. As mentioned in Sect. 4, the value of q^2 is conventionally chosen to be in the range $0.3 < q^2/{m_b}^2 < 0.5$. The CKM matrix, which should be determined from experimental data, is expressed in terms of the Wolfenstein parameters, A, λ_c, ρ, and η [20]. Here, we shall use the latest values [32], which were extracted from charmless semileptonic B decays ($|V_{ub}|$) charmed semileptonic B decays ($|V_{cb}|$) s and d mass oscillations, $\Delta m_s, \Delta m_d$, and CP violation in the kaon system (ϵ_K), (ρ, η). Hence, one has

$$\lambda_c = 0.2237\ ,\quad A = 0.8113\ ,\quad 0.190 < \rho < 0.268\ ,$$
$$0.284 < \eta < 0.366\ . \tag{61}$$

These values respect the unitarity triangle as well (see also Table 3). In our numerical simulations, we will use the average values of ρ and η.

5.1.2 Quark masses

The running quark masses are used in order to calculate the matrix elements of the penguin operators. The quark mass is evaluated at the scale $\mu \simeq m_b$ in the B decays. Therefore one has [33]

$$m_u(\mu = m_b) = 2.3\,\text{MeV}\ ,\quad m_d(\mu = m_b) = 4.6\ \text{MeV}\ ,$$
$$m_s(\mu = m_b) = 90\,\text{MeV}\ ,\quad m_b(\mu = m_b) = 4.9\,\text{GeV}, \tag{62}$$

which corresponds to $m_s(\mu = 1\,\text{GeV}) = 140\,\text{MeV}$. For the meson masses, we shall use the following values [13]:

$$\begin{aligned} m_{B^\pm} &= 5.279\ \text{GeV}\ ,\quad m_{K^{*0}} = 0.896\,\text{GeV}\ ,\\ m_\omega &= 0.782\,\text{GeV}\ ,\quad m_{B^0} = 5.279\,\text{GeV}\ ,\\ m_{\rho^\pm} &= 0.770\,\text{GeV}\ ,\quad m_{\pi^\pm} = 0.139\,\text{GeV}\ ,\\ m_{K^{*\pm}} &= 0.892\,\text{GeV}\ ,\quad m_{\rho^0} = 0.770\,\text{GeV}\ ,\\ m_{\pi^0} &= 0.135\,\text{GeV}\ . \end{aligned} \tag{63}$$

5.1.3 Form factors and decay constants

In Table 4 we list the relevant form factor values at zero momentum transfer [10,30,34] for the $B \to K^*$, $B \to \rho$ and $B \to \omega$ transitions. The different models are defined as follows: model (1) is the BSW model where the q^2 dependence of the form factors is described by a single-ansatz. Model (2) is the GH model with the same momentum dependence as model (1). Finally, we define the decay constant for the vector (f_V) meson as usually by

$$\begin{aligned} \sqrt{2}\langle\rho(q)|\bar{q}_1\gamma_\mu q_2|0\rangle &= f_\rho m_\rho \epsilon_\rho \ \text{ for } \rho \text{ and otherwise}\ ,\\ \langle V(q)|\bar{q}_1\gamma_\mu q_2|0\rangle &= f_V m_V \epsilon_V\ , \end{aligned} \tag{64}$$

Table 3. Values of the CKM unitarity triangle for limiting values of the CKM matrix elements

	α	β	γ
$(\rho_{\min}, \eta_{\min})$	104°47	19°32	56°21
$(\rho_{\min}, \eta_{\max})$	93°13	24°31	62°56
$(\rho_{\max}, \eta_{\min})$	112°14	21°20	46°66
$(\rho_{\max}, \eta_{\max})$	99°66	26°56	53°78

with q being the momentum of the vector meson and m_V and ϵ_V being the mass and polarization vector of the vector meson, respectively. Numerically, in our calculations, we take [13]

$$f_{K^*} = 214\,\text{MeV}\ ,\ f_\rho = 221\,\text{MeV}\ ,\ f_\omega = 195\,\text{MeV}\ . \tag{65}$$

Finally, the free parameter (effective number of color, $N_c^{\rm eff}$) is taken to lie between the lower (upper) limits 0.66 (2.84) for the $b \to s$ transition. Nevertheless, we focus our analysis on values of $N_c^{\rm eff}$ bigger than 1, as suggested in [35]. Regarding the $b \to d$ transition, the lower (upper) limits for $N_c^{\rm eff}$ are 0.98 (2.01) [35].

5.2 Simulation of the ρ^0–ω mixing

All the channels studied here include at least one ρ^0 meson which mixes with the ω meson. The other vector mesons are either a $K^{*0,\pm}$ or a $\rho^\pm$. Thus, the mass of each resonance is generated according to a relativistic Breit–Wigner expression:

$$\frac{\mathrm{d}\sigma}{\mathrm{d}M^2} = C_N \frac{\Gamma_R M_R}{\left(M^2 - M_R^2\right)^2 + \left(\Gamma_R M_R\right)^2}\ , \tag{66}$$

where C_N is a normalization constant. In (66), M_R and Γ_R are respectively the mass and the width of the vector meson which have been determined experimentally. M is the mass of the generated resonance. A simple and phenomenological relation describing the amplitude for ρ^0–ω mixing is used for the Monte Carlo simulations [36]. In the Breit–Wigner expression, the ρ^0-propagator is replaced by the following one:

$$\frac{1}{s_{\rho\omega}} = \frac{1}{s_\rho} + \frac{T_\omega}{T_\rho}\frac{\Pi_{\rho\omega}}{s_\rho s_\omega}\ , \tag{67}$$

where T_ω and T_ρ are respectively the ω and ρ production amplitudes. In addition, $\tilde{\Pi}_{\rho\omega}$ is the mixing parameter for which recent values come from $e^+e^- \to \pi^+\pi^-$ annihilations. Explanations have already been given in Sect. 3. Finally, $1/s_V$ has the same definition as in (22). Because the same physical processes enter the production of both the ρ^0 and ω resonances (they are both made out from $u\bar{u}$ and $d\bar{d}$ quark pairs with the same weight 1/2), it seems natural to choose $T_\omega/T_\rho = 1$. So the invariant mass distribution of the $\pi^+\pi^-$ system becomes simplified, being given by

$$\mathrm{d}\sigma/\mathrm{d}m^2 \propto \left|\mathcal{A}(\rho^0(\omega))\right|^2\ , \tag{68}$$

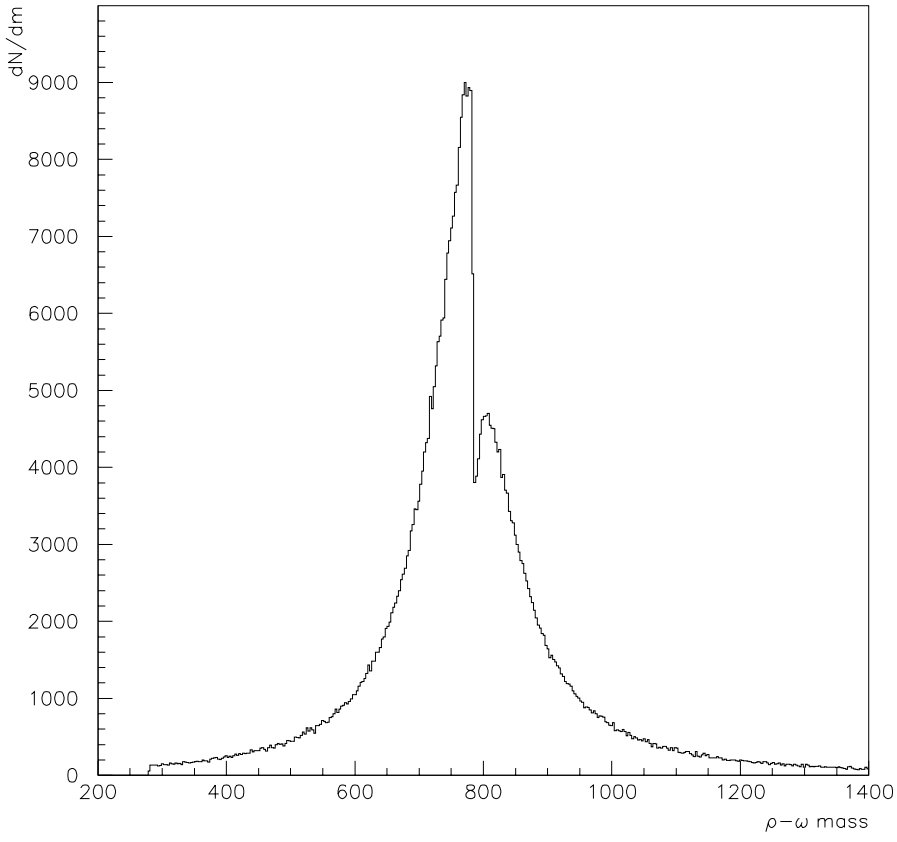

Fig. 4. Spectrum of ρ^0–ω mixing (in MeV/c^2), simulated by the interference of two Breit–Wigner curves

Table 4. Form factor values for $B \to \rho$, $B \to \omega$ and $B \to K^*$ at $q^2 = 0$ (see the reference in text)

			$B \to \rho$			
	h_V	$h_{A_0} = h_{A_3}$	h_{A_1}	h_{A_2}	m_V (GeV^2)	m_{A_i} (GeV^2)
model (1)	0.329	0.281	0.283	0.283	5.32	5.32
model (2)	0.394	0.345	0.345	0.345	5.32	5.32
			$B \to \omega$			
	h_V	$h_{A_0} = h_{A_3}$	h_{A_1}	h_{A_2}	m_V (GeV^2)	m_{A_i} (GeV^2)
model (1)	0.328	0.280	0.281	0.281	5.32	5.32
model (2)	0.394	0.345	0.345	0.345	5.32	5.32
			$B \to K^*$			
	h_V	$h_{A_0} = h_{A_3}$	h_{A_1}	h_{A_2}	m_V (GeV^2)	m_{A_i} (GeV^2)
model (1)	0.369	0.321	0.328	0.331	5.43	5.43
model (2)	0.443	0.360	0.402	0.416	5.43	5.43

where $\mathcal{A}(\rho^0(\omega))$ is the amplitude of the two mixed Breit–Wigner distributions and m is the $\pi^+\pi^-$ invariant mass. In Fig. 4, the $\pi^+\pi^-$ invariant mass spectra for ρ^0–ω mixing is displayed. Because of the very narrow width of ω, ($\Gamma_\omega = 8.44\,\text{MeV}$), we notice a high and narrow peak at the ω pole ($\approx 782\,\text{MeV}$).

5.3 Density matrix $h_{\lambda,\lambda'}$

Three main parameters remain free in our simulations: the ratio q^2/m_b^2 (related to the penguin diagrams), the form factor model (GH or BSW) and the effective number of colors, N_c^{eff} (associated with the factorization hypothesis). The histograms plotted in Fig. 5 display spectra of the diagonal and normalized density matrix elements $h_{i,i}$, for the channels $B^0 \to \rho^0(\omega)K^{*0}$ (left-hand side) and $B^+ \to \rho^0(\omega)\rho^+$ (right-hand side). The input numerical parameters are $q^2/m^2{}_b = 0.3$, $N_c^{\text{eff}} = 2.84$ (left-hand side figure) or $N_c^{\text{eff}} = 2.01$ (right-hand side figure), and the GH form factor model is applied for both decays. Note also that the average values of the CKM parameters ρ and η are used. The wide spectrum of values of the density matrix element $h_{\lambda,\lambda}$, is caused by the resonance widths (especially

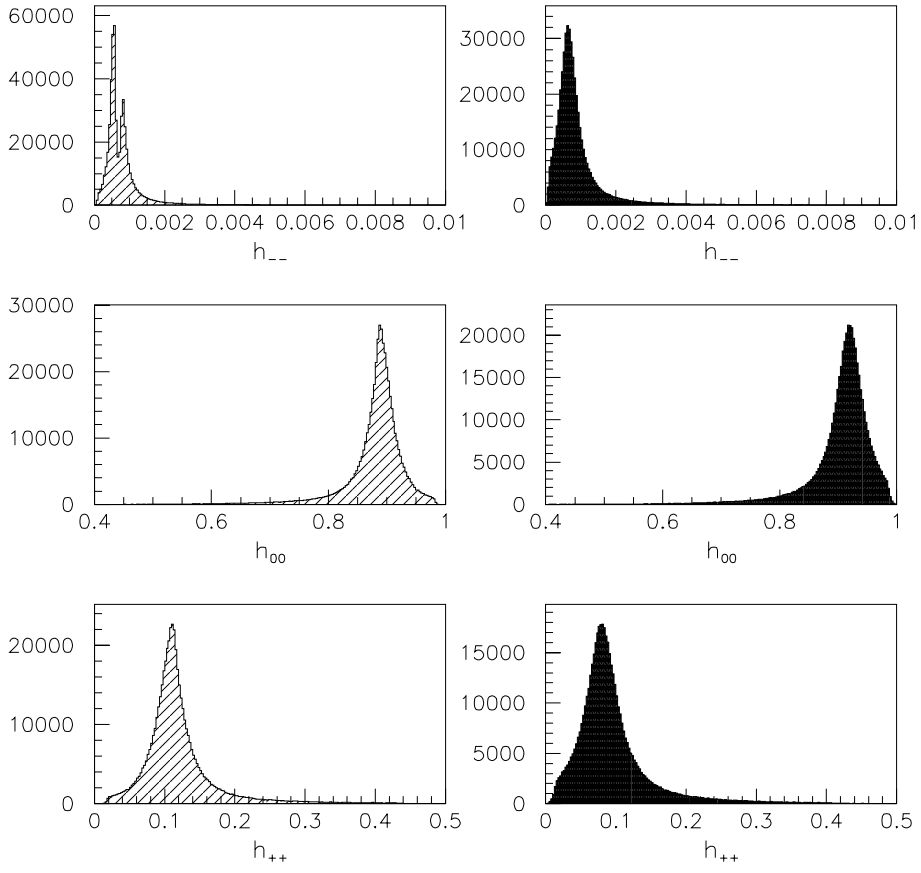

Fig. 5. Spectrum of h_{--}, h_{00}, h_{++}. Histograms on the left correspond to the channel $B^0 \to \rho^0(\omega)K^{*0}$ where the parameters used are $q^2/m^2{}_b = 0.3$, $N_c^{\rm eff} = 2.84$, $\rho = 0.229, \eta = 0.325$ and form factors from the GH model. Histograms on the right correspond to the channel $B^+ \to \rho^0(\omega)\rho^+$ for the same parameters with $N_c^{\rm eff} = 2.01$

that of the ρ) which provides, in turn, a large spectrum for the common momentum p_V in the B rest frame. Whatever the $\rho^0(\omega)V_2$ channel is, $h_{00} = |H_0|^2$, which corresponds to longitudinal polarization, is the dominant value. Numerically, for the $B^0 \to \rho^0(\omega)K^{*0}$ decay, the mean value of h_{00} is around 0.87, while it is of order 0.90 for $B^+ \to \rho^0(\omega)\rho^+$. The dominance of the longitudinal polarization has already been confirmed experimentally, since recent experimental data related to the channel $B \to J/\psi K^*$ show clearly that the longitudinal decay amplitude dominates in that case, with $|H_0|^2 = 0.59 \pm 0.06 \pm 0.01$ [37]. Extrapolating these results to the charmless vector meson final states requires some modifications of the form factors without a big change of the relative contributions of the polarization states. Regarding $h_{--} = |H_{-1}|^2$, it represents less than 0.5% of the total amplitude for both decays. This numerical result is confirmed by complete analytical calculations.

In Figs. 6 and 7, the real and imaginary parts of the non-diagonal and normalized density matrix elements $h_{i,j}$, are shown for the channels $B^0 \to \rho^0(\omega)K^{*0}$ and $B^+ \to \rho^0(\omega)\rho^+$, respectively. The input parameters are the same as previously mentioned. The main feature of the non-diagonal matrix elements, $h_{i,j}$, is the smallness of both the imaginary and real parts – the imaginary part being at least one order of magnitude smaller than the real part one. For the $B^+ \to \rho^0(\omega)\rho^+$ decay, we observe that the mean value of all the imaginary parts is zero, whereas it can vary for the other decay. Note also that the three real parts are quite similar for both decays. Because of the tiny value of $h_{--} = |H_{-1}|^2$, the moduli of the non-diagonal elements, $h_{+-} = H_+ H_-^*$ and $h_{0-} = H_0 H_-^*$, are very small, while the modulus of $h_{+0} = H_+ H_0^*$ is around 0.3 for both decays. As a first conclusion, the general behavior of the density matrix seems to be similar whatever the decay is. Experimentally, only the mean values of the diagonal elements and h_{+-} will one be able to measure through the angular distributions.

These angular distributions are plotted in Figs. 8 and 9 in the helicity frame and in the transversity frame, respectively for $B^0 \to \rho^0(\omega)K^{*0}$ and for the usual input parameters. Their normalized pdfs have been displayed above in (10). As a consequence of the small value of $\langle h_{+-} \rangle$, the azimuthal angle distribution in the helicity frame is nearly flat, whereas it is sinusoidal in the transversity frame. From the distribution as a function of polar angle (in the TF) displayed in (13), one can infer a mean value of the $H_{\rm T}$ amplitude. This represents an additional piece of information through which one can access the dynamics of $B(\bar{B})$ decays into two charmless hadrons.

6 Branching ratio and asymmetry in B decays into two vector mesons

The analytic expressions for the density matrix elements, h_{ij}, allow us to calculate the hadronic branching ratios

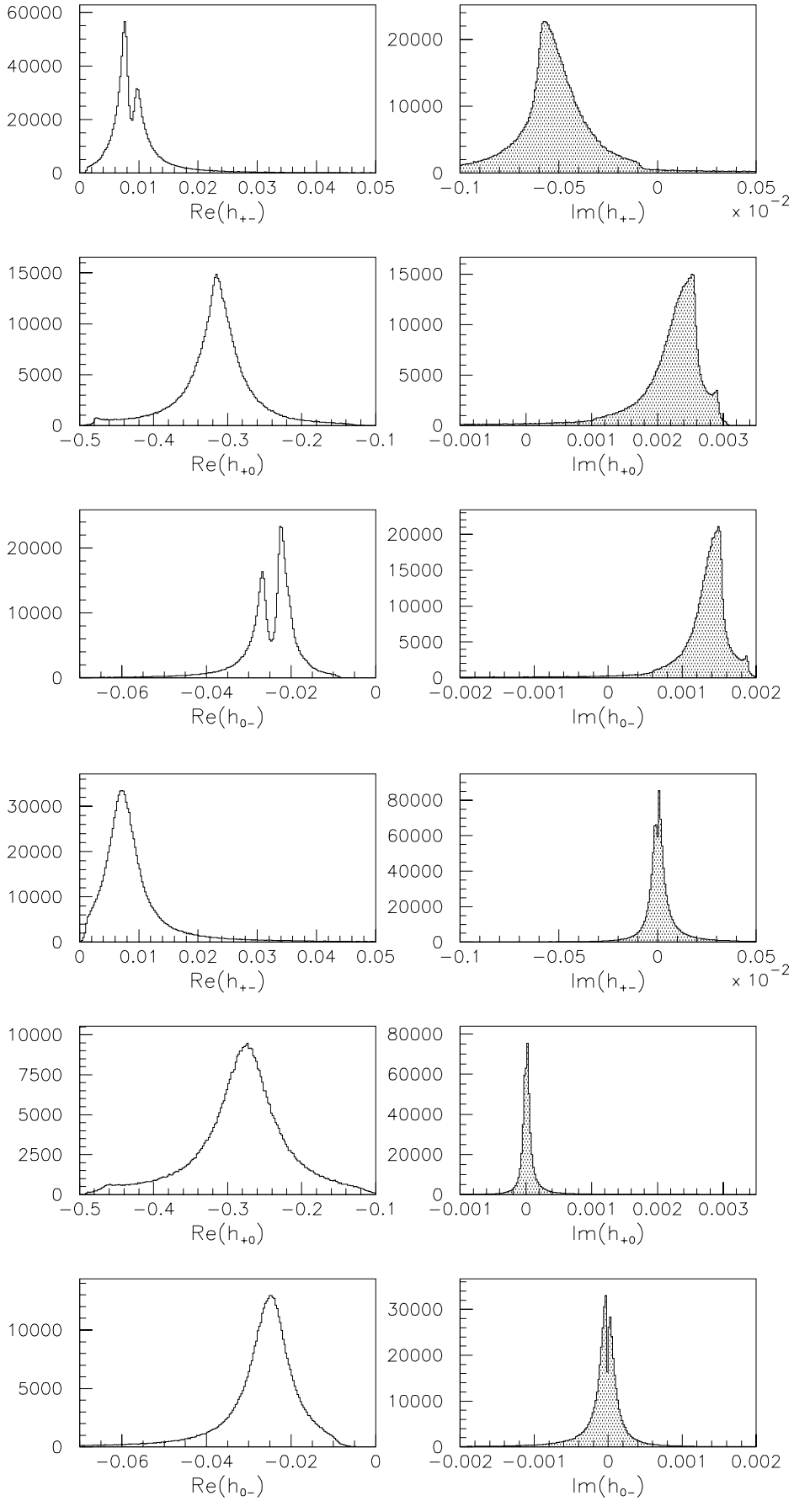

Fig. 6. Spectrum of $\mathrm{Re}(h_{ij})$ and $\mathrm{Im}(h_{ij})$ where $i \neq j$. Histograms correspond to channel $B^0 \to \rho^0(\omega)K^{*0}$ where the used parameters are $q^2/{m^2}_b = 0.3$, $N_c^{\mathrm{eff}} = 2.84$, $\rho = 0.229$, $\eta = 0.325$ and form factors from the GH model

Fig. 7. Spectrum of $\mathrm{Re}(h_{ij})$ and $\mathrm{Im}(h_{ij})$ where $i \neq j$. Histograms correspond to the channel $B^+ \to \rho^0(\omega)\rho^+$ where the used parameters are $q^2/{m^2}_b = 0.3$, $N_c^{\mathrm{eff}} = 2.01$, $\rho = 0.229$, $\eta = 0.325$ and form factors from the GH model

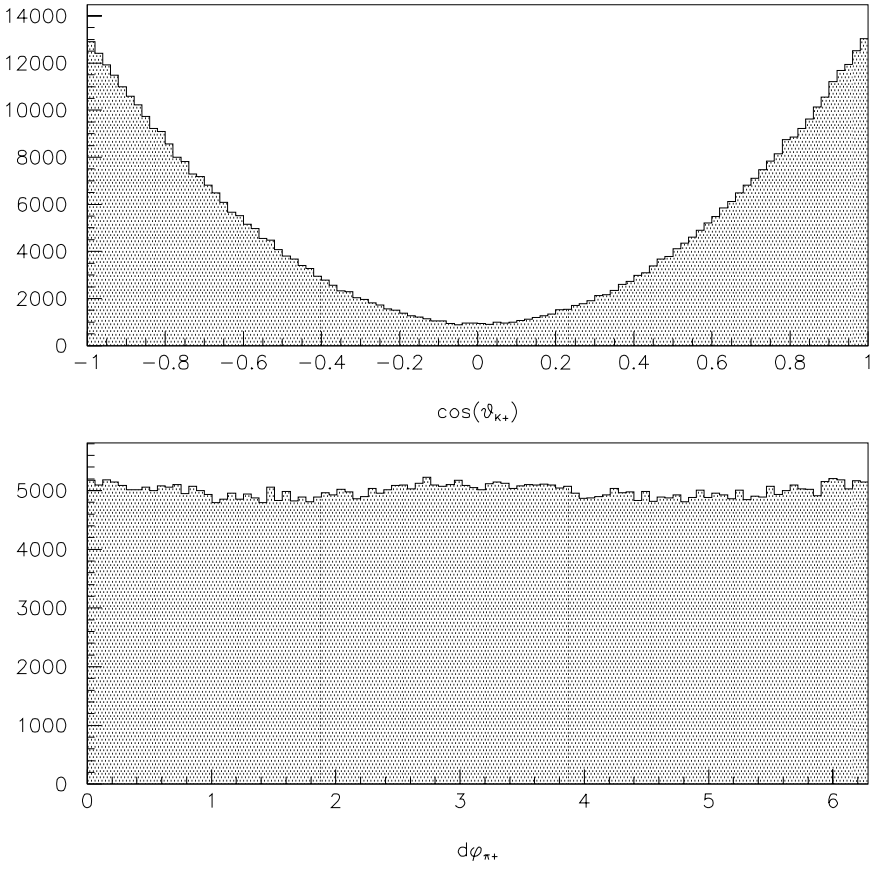

Fig. 8. Spectrum of polar angle (*upper figure*) and azimuthal angle (*lower one*) in the helicity frame for the channel $B^0 \to \rho^0(\omega)K^{*0}$. Parameters used are $q^2/m^2{}_b = 0.3$, $N_c^{\rm eff} = 2.84$, $\rho = 0.229, \eta = 0.325$ and form factors from the GH model

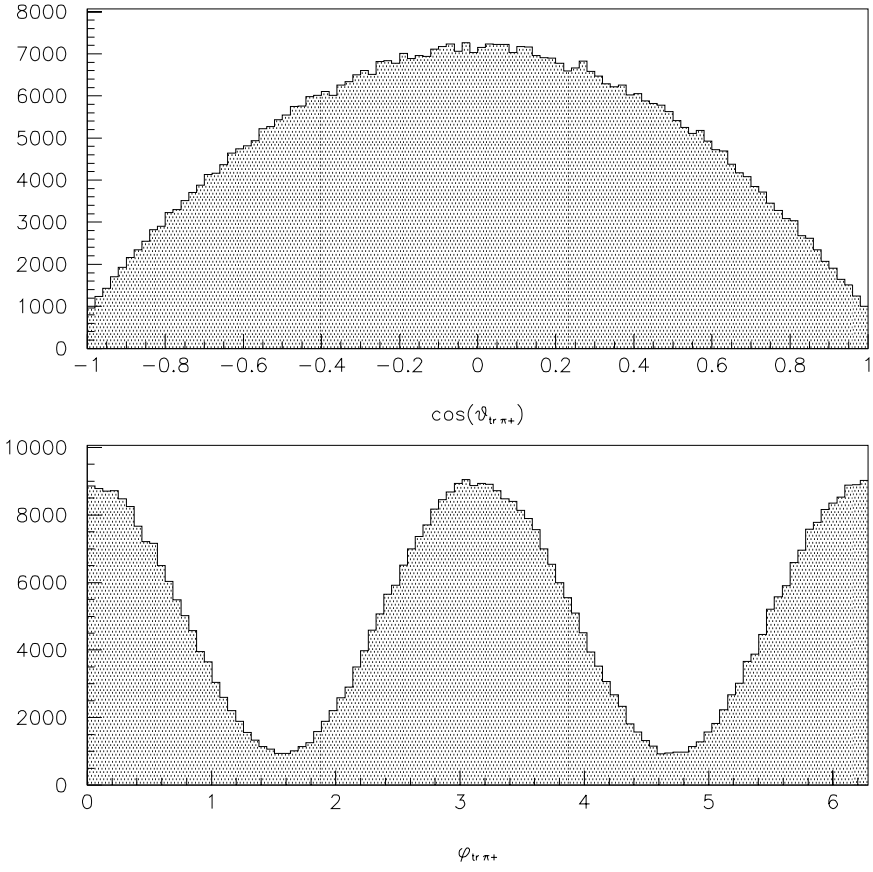

Fig. 9. Spectrum of the polar angle (*upper figure*) and the azimuthal angle (*lower one*) in the transversity frame for the channel $B^0 \to \rho^0(\omega)K^{*0}$. Parameters are $q^2/m^2{}_b = 0.3$, $N_c^{\rm eff} = 2.84$, $\rho = 0.229, \eta = 0.325$ and form factors from the GH model

Table 5. $\bar{B}^0, B^-$ branching ratios (in units of 10^{-6}) using either the BSW or GH form factor models, for $q^2/m_b^2 = 0.3$ (0.5), with $N_{\rm cmax}^{b\to s} = 2.84$ (2.82), $N_{\rm cmax}^{b\to d} = 2.01$ (1.95), $\rho = 0.229$ and $\eta = 0.325$

Channel	$\frac{q^2}{m_b^2}$	BSW	GH
$\bar{B}^0 \to \bar{K}^{*0}\rho^0(\omega)$	0.3	2.1	1.0
	0.5	1.5	0.73
$B^- \to K^{*-}\rho^0(\omega)$	0.3	6.6	3.9
	0.5	6.2	3.6
$B^- \to \rho^-\rho^0(\omega)$	0.3	24	13
	0.5	24	14

Table 6. B^0, B^+ branching ratios (in units of 10^{-6}) using either the BSW or GH form factor models, for $q^2/m_b^2 = 0.3$ (0.5), with $N_{\rm cmax}^{b\to s} = 2.84$ (2.82), $N_{\rm cmax}^{b\to d} = 2.01$ (1.95), $\rho = 0.229$ and $\eta = 0.325$

Channel	$\frac{q^2}{m_b^2}$	BSW	GH
$B^0 \to K^{*0}\rho^0(\omega)$	0.3	2.1	1.0
	0.5	1.7	0.83
$B^+ \to K^{*+}\rho^0(\omega)$	0.3	5.8	3.4
	0.5	3.8	2.3
$B^+ \to \rho^+\rho^0(\omega)$	0.3	20	11
	0.5	20	11

$\mathcal{B}(B \to \rho^0(\omega)V_2)$ and to estimate the asymmetries related to the B and $\bar{B}$ decays. All these physical observables depend primarily on a subset of the parameters mentioned previously, such as the form factors, the ratio $q^2/{m_b}^2$ (where q^2 is the mass of the virtual gluon in the penguin diagram), the effective number of colors, $N_c^{\rm eff}$ (used as a free parameter in the framework of the factorization hypothesis), and the CKM matrix element parameters ρ and η.

6.1 Branching ratio: results and discussions

Departing from the definition of the branching ratio ($\mathcal{B}(B \to f)$),

$$\mathcal{B}(B \to f) = \frac{\Gamma(B \to f)}{\Gamma(B \to \text{All})} \ , \tag{69}$$

the width $\Gamma(B \to V_1V_2)$ can be inferred from its differential form given by the standard relation [38]:

$$\begin{aligned} &\mathrm{d}\Gamma(B \to V_1V_2) \qquad (70)\\ &= \frac{1}{8\pi^2 M}\ |\mathcal{M}(B \to V_1V_2)|^2\ \frac{\mathrm{d}^3\vec{p}_1}{2E_1}\ \frac{\mathrm{d}^3\vec{p}_2}{2E_2}\ \delta^4(P - p_1 - p_2)\ . \end{aligned}$$

In (70), $P = (M, \vec{0})$, where $M = m_b$ and $(E_1, \vec{p}_1)$ and $(E_2, \vec{p}_2)$ are the four-momenta of V_1 and V_2, respectively, in the B rest frame. Because of the large width of the ρ^0 meson ($\Gamma_\rho \approx 150\,\text{MeV}$) and the K^* meson ($\Gamma_{K^*} \approx 50\,\text{MeV}$), the energy, E_i, and the momentum, p_i, of each vector meson vary according to the generated event. Computation of $\Gamma(B \to \rho^0(\omega)V_2)$ could not be done analytically but numerically by Monte Carlo methods. A total number of 50 000 events have been generated in order to obtain a precise estimate of this decay width.

In Tables 5 and 6 we list (respectively) the branching ratios for $\bar{B} \to \rho^0(\omega)\bar{V}_2$ and $B \to \rho^0(\omega)V_2$ and their dependence on the form factor models (BSW and GH), q^2/m_b^2, $N_c^{\rm eff}$ and the average values of the CKM parameters ρ and η. For a fixed value of $q^2/{m_b}^2$, there are important variations of the branching ratios, depending on the form factor model. They can vary by up to a factor two. In the framework of a given form factor model, some branching ratio modifications appear with $q^2/{m_b}^2$, especially in the channels including a K^*. However, these changes do not exceed 34%. Regarding the ratio between $\mathcal{B}(B^0 \to \rho^0(\omega)K^{*0})$ and $\mathcal{B}(B^+ \to \rho^0(\omega)K^{*+})$, its value is found to be of the order of 0.40 for the BSW model and 0.34 for the GH model.

The relative difference between the two conjugate branching ratios $\mathcal{B}(B \to f)$ and $\mathcal{B}(\bar{B} \to \bar{f})$ is almost independent of the form factor models, for a fixed value of $q^2/{m_b}^2$. It can be computed from the two tables just mentioned and, usually, it does not exceed 20%. The exception is for the $K^{*\pm}\rho^0(\omega)$ channels, where it reaches 39%.

6.2 Asymmetry: results and discussions

A search for direct CP violation requires asymmetries between conjugate final states coming from the B and $\bar{B}$ decays respectively. In our case, these searches are performed in two complementary ways. We consider first the global CP-violating asymmetry a_{CP}, calculated from the branching ratios:

$$a_{CP} = \frac{\mathcal{B}(B \to f) - \overline{\mathcal{B}}(\bar{B} \to \bar{f})}{\mathcal{B}(B \to f) + \overline{\mathcal{B}}(\bar{B} \to \bar{f})}\ . \tag{71}$$

Secondly, we use the partial widths of $B(\to f)$ and $\bar{B}(\to \bar{f})$, calculated as described above together with the differential asymmetries investigated as a function of the $\pi^+\pi^-$ invariant mass in the whole range of the ρ^0 Breit–Wigner resonance. Hence, $a_{CP}(m)$ takes the following form:

$$a_{CP}(m) = \frac{\Gamma_m(B \to f) - \bar{\Gamma}_m(\bar{B} \to \bar{f})}{\Gamma_m(B \to f) + \bar{\Gamma}_m(\bar{B} \to \bar{f})}\ , \tag{72}$$

where m is the $\pi^+\pi^-$ invariant mass. $\Gamma_m(B \to f)$ and $\bar{\Gamma}_m(\bar{B} \to \bar{f})$ in (72) are the partial widths written as a function of m.

In Table 7 we list the global CP-violating asymmetry between the B and $\bar{B}$ decays for the channels under investigation. It can be noticed that, for a fixed value of $q^2/{m_b}^2$, the two form factor models provide quite similar results. For different $q^2/{m_b}^2$ values, the corresponding results could vary, especially in the $K^{*\pm}\rho^0(\omega)$ channels. In Figs. 10 and 11 we show, respectively, the histogram of

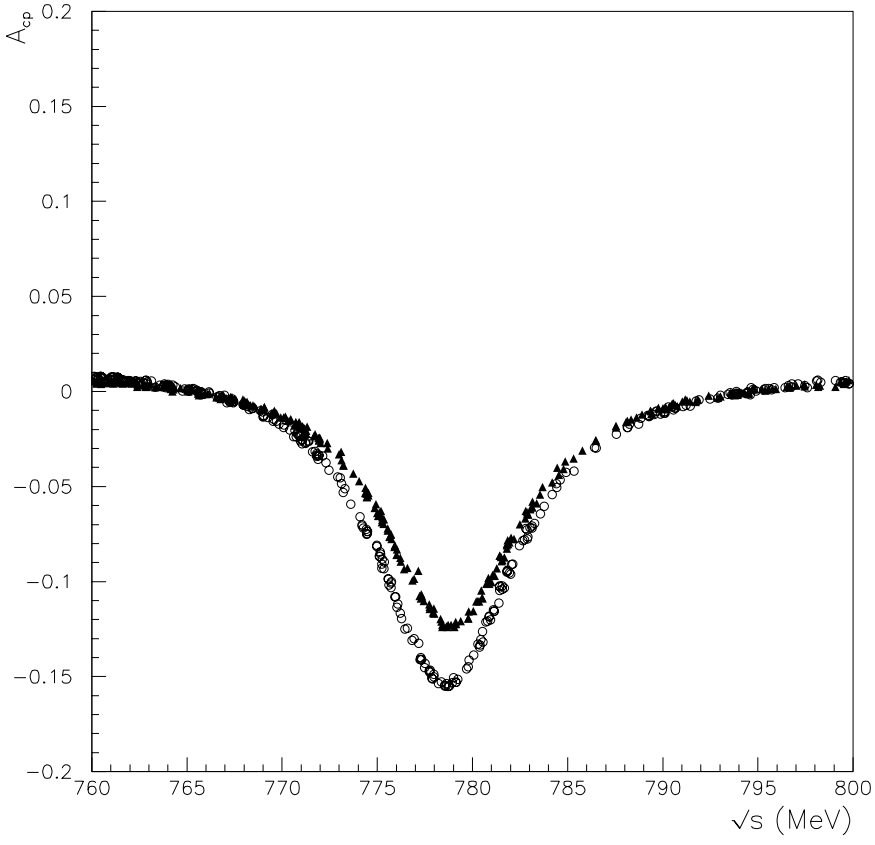

Fig. 10. CP-violating asymmetry parameter $a_{CP}(m)$, as a function of the $\pi^+\pi^-$ invariant mass in the vicinity of the ω mass region for the channel $B^0 \to \rho^0(\omega)K^{*0}$. Parameters are $q^2/{m^2}_b = 0.3$, $N_c^{\rm eff} = 2.84$, $\rho = 0.229, \eta = 0.325$. Solid triangles up and circles correspond to the BSW and GH form factor models respectively

Table 7. Global CP-violating asymmetries (in percents) using either the BSW or GH form factor models, for $q^2/m_b^2 = 0.3$ (0.5), with $N_{\rm cmax}^{b\to s} = 2.84$ (2.82), $N_{\rm cmax}^{b\to d} = 2.01(1.95)$, $\rho = 0.229$ and $\eta = 0.325$

Channel	$\frac{q^2}{m_b^2}$	BSW	GH
$\bar{K}^{*0}(K^{*0})\rho^0(\omega)$	0.3	+0.36	−0.45
	0.5	+4.70	+5.90
$K^{*-}(K^{*+})\rho^0(\omega)$	0.3	−6.6	−6.37
	0.5	−23.0	−22.0
$\rho^-(\rho^+)\rho^0(\omega)$	0.3	−8.5	−9.6
	0.5	−8.7	−9.9

the direct CP-violating asymmetry parameter $a_{CP}(m)$, for the decays $B^0 \to \rho^0(\omega)K^{*0}$ and $B^+ \to \rho^0(\omega)\rho^+$, as a function of the $\pi^+\pi^-$ invariant mass in the ω mass region and for both form factor models. The asymmetry reaches its maximum when $\sqrt{s}$ is around 780 MeV. However, outside the displayed windows, the asymmetry goes to zero in any case. The peak of the asymmetry is emphasized when the GH form factor model is used in our simulations. For the $K^{*0}\rho^0(\omega)$ channels, the maximum of the CP violating asymmetry is around 13% and 16%, for the BSW model and the GH model, respectively. Finally, we emphasize that the $\rho^\pm\rho^0(\omega)$ channels present the most intriguing results because, in any case, their asymmetry is at least 80% (BSW model) and can reach 95% (GH model). This last channel is highly recommended for a direct search for CP violation.

7 Perspectives and conclusions

We have studied direct CP violation in decay process such as $B \to \rho^0(\omega)V_2 \to \pi^+\pi^- V_2$, where V_2 is either $K^{*0,\pm}$ or $\rho^\pm$, with the inclusion of ρ^0–ω mixing. When the invariant mass of the $\pi^+\pi^-$ pair is in the vicinity of the ω resonance, it is found that the CP-violating asymmetry, $a_{CP}(m)$, reaches its maximum value. In our analysis we have also investigated the branching ratios for the same channels. Thanks to the standard helicity and transversity formalisms, rigorous and detailed calculations of the $B^{0\pm}$ decays into two charmless vector mesons have been carried out completely. Using the effective Hamiltonian based on the operator product expansion with the appropriate Wilson coefficients, we derived in detail the amplitudes corresponding to $B \to \rho^0(\omega)V_2 \to \pi^+\pi^- V_2$ decay and the density matrix, $h_{\lambda\lambda'}$ as well.

In order to apply our formalism, we used a Monte Carlo method for all the numerical simulations. Moreover, we dealt at length with the uncertainties coming from the input parameters. In particular, these include the Cabibbo–Kobayashi–Maskawa matrix element parameters, ρ and η, the effective number of colors, $N_c^{\rm eff}$, coming from the naive factorization and two phenomenological models in order to show the possible dependence on the form factors, GH or

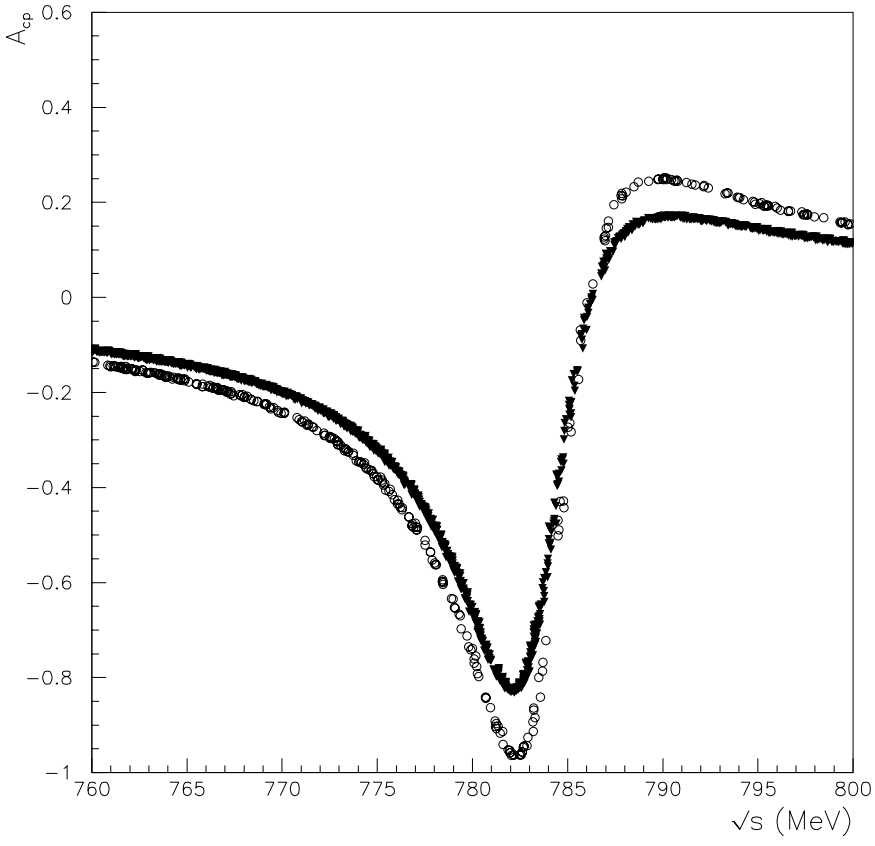

Fig. 11. CP-violating asymmetry parameter $a_{CP}(m)$, as a function of the $\pi^+\pi^-$ invariant mass in the vicinity of the ω mass region for the channel $B^+ \to \rho^0(\omega)\rho^+$. Parameters are $q^2/m^2{}_b = 0.3$, $N_c^{\rm eff} = 2.01$, $\rho = 0.229, \eta = 0.325$. Solid triangles down and circles correspond to the BSW and GH form factor models respectively

BSW. These form factors vary slightly according to the final states. Recall that this work was achieved by applying a phenomenological treatment, where some assumptions regarding the evaluation of the hadronic matrix elements have been made. In this approach, corrections associated with the limit of validity of the factorization hypothesis were parameterized phenomenologically and may involve large uncertainties.

As a major result, the predominance of the longitudinal polarization, h_{00}, has been pointed out in all the investigated decays. We also found a large direct CP-violating asymmetry in these B decays into two charmless vector mesons. We stress that, without the inclusion of ρ^0–ω mixing, we would not have a large CP-violating asymmetry. Finally, we predicted branching ratios to be of the order 0.7–2.1×10^{-6} for $K^{*0}\rho^0(\omega)$ and of the order 2.3–6.6×10^{-6} for $K^{*\pm}\rho^0(\omega)$ (depending on the different phenomenological models). For the channel $\rho^\pm\rho^0(\omega)$, we found the branching ratios to be of the order 11–24×10^{-6}.

Two main conclusions can be drawn. The first is the relative importance of the form factor model which is used, since some branching ratios in $B \to \rho^0(\omega)V_2$ could change by up to a factor two. The second is the important role of ρ^0–ω mixing, which can considerably enhance the asymmetry parameter a_{CP}, between the conjugate final states coming, respectively, from B and $\bar{B}$ decays.

Beside the "standard" ways to look for direct CP violation, such as the difference between branching ratios and/or discrepancies in the angular distributions of the decay products, we have presented a detailed discussion of a new method. This involves the variation of a_{CP} as a function of the $\pi^+\pi^-$ invariant mass over the whole range of the ρ^0 resonance [12,35]. We believe that this method will be very fruitful for future experiments and has already been implemented in the generator of the LHCb experiment. Indeed, we look forward to being able to apply the formalism developed here to the analysis of experimental data for decays such as $B \to \rho^0(\omega)V_2$ (with V_2 being either a K^* or a $\rho^\pm$) in the near future.

Acknowledgements. This work was supported in part by the Australian Research Council and the University of Adelaide. The LHCb Clermont-Ferrand group would like to acknowledge G. Menessier from the LPTM, for many illuminating discussions regarding the exciting question of FSI in hadronic physics.

Appendix

A Practical calculations of the helicity amplitudes

The helicity formalism in the case of vector mesons requires the introduction of three polarization four-vectors for each spin-1 particle [39]:

$$\epsilon(1) = (0, \vec{\epsilon}(1)) \ , \quad \epsilon(2) = (0, \vec{\epsilon}(2)) \ ,$$

and

$$\epsilon(3) = \left(|\vec{k}|/m, E\hat{k}/m\right) . \quad (73)$$

They satisfy the following relations as well:

$$\epsilon(i)^2 = -1 \ , \text{ and } \ \epsilon(i)\cdot\epsilon(j) = 0 \ , \quad \text{with } i \neq j \ , \quad (74)$$

where m, E and $\vec{k}$ are respectively the mass, the energy and the momentum of the vector meson. $\hat{k}$ is defined as the unit vector along the vector momentum, $\hat{k} = \vec{k}/|\vec{k}|$. The three vectors $\vec{\epsilon}(1), \vec{\epsilon}(2)$ and $\vec{\epsilon}(3) = E\hat{k}/m$ form an orthogonal basis. $\vec{\epsilon}(1)$ and $\vec{\epsilon}(2)$ are the *transverse polarization* vectors while $\vec{\epsilon}(3)$ is the *longitudinal polarization* vector. These three vectors allow one to define the *helicity basis*:

$$\epsilon(+) = \frac{(\epsilon(1) + \mathrm{i}\,\epsilon(2))}{\sqrt{2}} \ , \quad \epsilon(-) = \frac{(\epsilon(1) - \mathrm{i}\,\epsilon(2))}{\sqrt{2}} \ ,$$

and

$$\epsilon(0) = \epsilon(3) \ . \quad (75)$$

These four-vectors are *eigenvectors* of the helicity operator $\mathcal{H}$ corresponding, respectively, to the eigenvalues $\lambda = +1, -1$ and 0. In the $B^{0\pm}$ rest frame, the vector mesons have opposite momentum $\vec{k}_1 = -\vec{k}_2$ and their respective polarization vectors are *correlated*. This implies the following expressions:

$$\vec{k}_K = -\vec{k}_\rho = \vec{k} = \begin{pmatrix} k\sin\theta\cos\phi \\ k\sin\theta\sin\phi \\ k\cos\theta \end{pmatrix} \ ,$$

where θ and ϕ are respectively the polar and azimuthal angles of the produced K^*. In our case, one has for the transversal polarization vectors (K^* and ρ) the expressions

$$\vec{\epsilon}_K(1) = \begin{pmatrix} \cos\theta\cos\phi \\ \cos\theta\sin\phi \\ -\sin\theta \end{pmatrix} = \vec{\epsilon}_\rho(1) \ ,$$

and

$$\vec{\epsilon}_K(2) = \begin{pmatrix} -\sin\phi \\ \cos\phi \\ 0 \end{pmatrix} = -\vec{\epsilon}_\rho(2) \ .$$

Regarding the longitudinal polarization, $\epsilon_K(3)$ and $\epsilon_\rho(3)$ take the form

$$\epsilon_K(3) = \left(\frac{|\vec{k}|}{m_K}, \frac{E_K}{m_K}\hat{k}\right) \ , \quad \epsilon_\rho(3) = \left(\frac{|\vec{k}|}{m_\rho}, \frac{E_\rho}{m_\rho}(-\hat{k})\right) \ . \quad (76)$$

By applying the relations from (75), one can express the vectors $\vec{\epsilon}(i)$ in the helicity basis and one gets $\vec{\epsilon}(\pm)$:

$$\vec{\epsilon}_K(+) = \begin{pmatrix} \cos\theta\cos\phi - \mathrm{i}\sin\phi \\ \cos\theta\sin\phi + \mathrm{i}\cos\phi \\ -\sin\theta \end{pmatrix} /\sqrt{2} = \vec{\epsilon}_K^{\,*}(-) = \vec{\epsilon}_\rho(-) \ , \quad (77)$$

$$\vec{\epsilon}_K(-) = \begin{pmatrix} \cos\theta\cos\phi + \mathrm{i}\sin\phi \\ \cos\theta\sin\phi - \mathrm{i}\cos\phi \\ -\sin\theta \end{pmatrix} /\sqrt{2} = \vec{\epsilon}_K^{\,*}(+) = \vec{\epsilon}_\rho(+) \ . \quad (78)$$

The weak hadronic amplitude is therefore decomposed, in the helicity basis, according to the general method developed by Bauer, Stech and Wirbel [10]. This will allow one to obtain two interesting results. Firstly, one can isolate the contribution of each helicity state to the total amplitude. Secondly, the contributions of the *tree* and *penguin* operators to the total amplitude can be separated via the helicity states.

The knowledge of the main input parameters ρ, η, A, $\sin\theta_c (= \lambda_c)$ and the masses and widths of the intermediate resonances allow one to make a complete determination of the three helicity amplitudes $H_\lambda\left(B \to \rho^0(\omega)V_2\right)$, where the helicity λ can take the values $-1, 0$ or $+1$.

B Channel $B^\pm \to \rho^0(\omega)\rho^\pm$

The formalism applied in case of $B \to \rho^0(\omega)K^*$ can be extended to $B^\pm \to \rho^0(\omega)\rho^\pm$. Nevertheless, in the last case one has a $b \to d$ transition instead of $b \to s$. The amplitude $H_\lambda\left(B \to \rho^0(\omega)V_2\right)$ has the form

$$\begin{aligned} &H_{\lambda=^0_{\pm1}}\left(B \to \rho^0(\omega)V_2\right) \\ &= A\lambda^3 \Bigg\{ \left[R_1^\rho B^\rho_{\lambda=^0_{\pm1}} + R_2^\rho C^\rho_{\lambda=^0_{\pm1}}\right] \\ &+ \mathrm{i}\left[I_1^\rho B^\rho_{\lambda=^0_{\pm1}} + I_2^\rho C^\rho_{\lambda=^0_{\pm1}}\right] \Bigg\} \\ &+ \frac{\tilde{\Pi}_{\rho\omega}}{(s_\rho - m_\omega^2) + \mathrm{i}m_\omega\Gamma_\omega} \Big[A\lambda^3 \Big\{ \left[R_1^\omega B^\omega_{\lambda=^0_{\pm1}} + R_2^\omega C^\omega_{\lambda=^0_{\pm1}}\right] \\ &\quad + \mathrm{i}\left[I_1^\omega B^\omega_{\lambda=^0_{\pm1}} + I_2^\omega C^\omega_{\lambda=^0_{\pm1}}\right]\Big\}\Big] \ , \end{aligned} \quad (79)$$

where one defines

$$R_i^{V_1} = \left(1 - \frac{\lambda^2}{2}\right)\eta c_{t_i}^{V_1} + \eta\ \mathrm{Re}(c_{p_i}^{V_1}) - (1-\rho)\ \mathrm{Im}(c_{p_i}^{V_1}), \quad (80)$$

$$I_i^{V_1} = \left(1 - \frac{\lambda^2}{2}\right)\rho c_{t_i}^{V_1} + \eta\ \mathrm{Im}(c_{p_i}^{V_1}) + (1-\rho)\ \mathrm{Re}(c_{p_i}^{V_1}), \quad (81)$$

with V_1 being either ρ^0 or ω. We have

$$\text{if } \ V_1 \equiv \rho \text{ and } i = 2 \text{ then } R_i^{V_1} = I_i^{V_1} = 0 \ . \quad (82)$$

The expressions for $c_{t_i}^{V_1}$ and $c_{p_i}^{V_1}$, which correspond to the investigated channel, take the following form.

(1) For the decay $B^- \to \rho^0\rho^-$:

$$\begin{aligned} c_{t_1}^\rho &= C_1' + \frac{C_2'}{N_c} + C_2' + \frac{C_1'}{N_c} \ , \\ c_{p_1}^\rho &= \frac{3}{2}\left(C_7' + \frac{C_8'}{N_c} + C_9' + \frac{C_{10}'}{N_c} + C_{10}' + \frac{C_9'}{N_c}\right) \ . \end{aligned} \quad (83)$$

(2) In the case of ω production, one obtains the linear combinations of the effective Wilson coefficients for the decay $B^- \to \omega\rho^-$:

$$
\begin{aligned}
c^{\omega}_{t_1} &= C'_2 + \frac{C'_1}{N_c}\ , \quad c^{\omega}_{p_1} = C'_4 + \frac{C'_3}{N_c} + \left(C'_{10} + \frac{C'_9}{N_c}\right)\ , \\
c^{\omega}_{t_2} &= C'_1 + \frac{C'_2}{N_c}\ , \\
c^{\omega}_{p_2} &= 2\left(C'_3 + \frac{C'_4}{N_c} + C'_5 + \frac{C'_6}{N_c}\right) \\
&\quad + \frac{1}{2}\left(C'_9 + \frac{C'_{10}}{N_c} + C'_7 + \frac{C'_8}{N_c} - C'_{10} - \frac{C'_9}{N_c}\right)\ . \qquad (84)
\end{aligned}
$$

All the terms used in the appendix have been defined in Sect. 4.

References

1. A.B. Carter, A.I. Sanda, Phys. Rev. Lett. **45**, 952 (1980); Phys. Rev. D **23**, 1567 (1981); I.I. Bigi, A.I. Sanda, Nucl. Phys. B **193**, 85 (1981)
2. Proceedings of the Workshop on CP Violation, Adelaide 1998, edited by X.-H. Guo, M. Sevior, A.W. Thomas (World Scientific, Singapore)
3. A. Bozek (BELLE Collaboration), in Proceedings of the 4th International Conference on B Physics and CP Violation, Ise-Shima, Japan, February 2001, hep-ex/0104041; K. Abe et al. (BELLE Collaboration), in Proceedings of the XX International Symposium on Lepton and Photon Interactions at High Energies, July 2001, Roma, Italy, BELLE-CONF-0115 (2001); K. Abe et al. (BELLE Collaboration), Phys. Rev. D **65**, 092005 (2002); R.S. Lu et al. (BELLE Collaboration), Phys. Rev. Lett. **89**, 191801 (2002)
4. T. Schietinger (BABAR Collaboration), Proceedings of Lake Louise Winter Institute on Fundamental Interactions, Alberta, Canada, February 2001, hep-ex/0105019; B. Aubert et al. (BABAR Collaboration), hep-ex/0008058; B. Aubert et al. (BABAR Collaboration), Phys. Rev. Lett. **87**, 221802 (2001)
5. I. Dunietz et al., Phys. Rev. D **43**, 2193 (1991)
6. M.E. Rose, Elementary theory of angular momentum (Dover)
7. A. Bohr, Nuclear Physics **10**, 486 (1959)
8. H. Quinn, Hadronic effects in two-body B decays. Lectures at SLAC Summer Institute (1999)
9. J. Schwinger, Phys. Rev. **12**, 630 (1964); D. Farikov, B. Stech, Nucl. Phys. B **133**, 315 (1978); N. Cabibbo, L. Maiani, Phys. Lett. B **73**, 418 (1978); M.J. Dugan, B. Grinstein, Phys. Lett. B **255**, 583 (1991)
10. M. Bauer, B. Stech, M. Wirbel, Z. Phys. C **34**, 103 (1987); M. Wirbel, B. Stech, M. Bauer, Z. Phys. C **29**, 637 (1985)
11. M. Beneke, G. Buchalla, M. Neubert, C.T. Sachrajda, Nucl. Phys. B **591**, 313 (2000)
12. S. Gardner, H.B. O'Connell, A.W. Thomas, Phys. Rev. Lett. **80**, 1834 (1998) [hep-ph/9705453]
13. The Particle Data Group, D.E. Groom et al., Eur. Phys. J. C **15**, 1 (2000)
14. J.J. Sakurai, Currents and mesons (University of Chicago Press 1969)
15. H.B. O'Connell, B.C. Pearce, A.W. Thomas, A.G. Williams, Prog. Part. Nucl. Phys. **39**, 201 (1997); H.B. O'Connell, A.G. Williams, M. Bracco, G. Krein, Phys. Lett. B **370**, 12 (1996); H.B. O'Connell, Aust. J. Phys. **50**, 255 (1997)
16. S. Gardner, H.B. O'Connell, A.W. Thomas, Phys. Rev. Lett. **80**, 1834 (1998)
17. X.-H. Guo, A.W. Thomas, Phys. Rev. D **58**, 096013 (1998); Phys. Rev. D **61**, 116009 (2000)
18. H.B. O'Connell, A.W. Thomas, A.G. Williams, Nucl. Phys. A **623**, 559 (1997); K. Maltman, H.B. O'Connell, A.G. Williams, Phys. Lett. B **376**, 19 (1996)
19. S. Gardner, H.B. O'Connell, Phys. Rev. D **57**, 2716 (1998)
20. L. Wolfenstein, Phys. Rev. Lett. **51**, 1945 (1983); Phys. Rev. Lett. **13**, 562 (1964)
21. A.J. Buras, Lect. Notes Phys. **558**, 65 (2000); also in Recent Developments in Quantum Field Theory, edited by P. Breitenlohner, D. Maison, J. Wess (Springer-Verlag, Berlin, in press), hep-ph/9901409
22. V.A. Novikov, M.A. Shifman, A.I. Vainshtein, V.I. Zakharov, Nucl. Phys. B **249**, 445 (1985); Yad. Fiz. **41**, 1063 (1985)
23. M.A. Shifman, A.I. Vainshtein, V.I. Zakharov, Nucl. Phys. B **147**, 385 (1979); Nucl. Phys. B **147**, 448 (1979)
24. A.J. Buras, in Probing the Standard Model of Particle Interactions (Elsevier Science, 1998), hep-ph/9806471
25. N.G. Deshpande, X.-G. He, Phys. Rev. Lett. **74**, 26 (1995)
26. R. Fleischer, Int. J. Mod. Phys. A **12**, 2459 (1997); Z. Phys. C **62**, 81 (1994); Z. Phys. C **58**, 483 (1993)
27. G. Kramer, W. Palmer, H. Simma, Nucl. Phys. B **428**, 77 (1994)
28. R. Enomoto, M. Tanabashi, Phys. Lett. B **386**, 413 (1996)
29. G. Buchalla, A.J. Buras, M.E. Lautenbacher, Rev. Mod. Phys. **68**, 1125 (1996)
30. X.-H. Guo, T. Huang, Phys. Rev. D **43**, 2931 (1991)
31. Y.-H. Chen, H.-Y. Cheng, B. Tseng, K.-C. Yang, Phys. Rev. D **60**, 094014 (1999)
32. By ALEPH, CDF, DELPHI, L3, OPAL and SLD Collaborations (D. Abbaneo et al.), hep-ex/0112028
33. H.-Y. Cheng, A. Soni, Phys. Rev. D **64**, 114013 (2001)
34. D. Melikhov, B. Stech, Phys. Rev. D **62**, 014006 (2000)
35. O. Leitner, X.-H. Guo, A.W. Thomas, Phys. Rev. D **66**, 096008 (2002); X.-H. Guo, O. Leitner, A.W. Thomas, Phys. Rev. D **63**, 056012 (2001)
36. P. Langacker, Phys. Rev. D **20**, 2983 (1979)
37. T. Affolder et al., Phys. Rev. Let. **85**, 4668 (2000) and references therein
38. J.D. Jackson, Il Nuovo Cimento, **34**, 1644 (1964)
39. De Wit, J. Smith, Field theory in particle physics (North-Holland 1986)